BAMS Article

Sea2Cloud

From Biogenic Emission Fluxes to Cloud Properties in the Southwest Pacific

Karine Sellegri, Mike Harvey, Maija Peltola, Alexia Saint-Macary, Theresa Barthelmeß, Manon Rocco, Kathryn A. Moore, Antonia Cristi, Frederic Peyrin, Neill Barr, Laurent Labonnote, Andrew Marriner, John McGregor, Karl Safi, Stacy Deppeler, Stephen Archer, Erin Dunne, James Harnwell, Julien Delanoe, Evelyn Freney, Clémence Rose, Clément Bazantay, Céline Planche, Alfonso Saiz-Lopez, Jesús E. Quintanilla-López, Rosa Lebrón-Aguilar, Matteo Rinaldi, Sandra Banson, Romain Joseph, Aurelia Lupascu, Olivier Jourdan, Guillaume Mioche, Aurélie Colomb, Gus Olivares, Richard Querel, Adrian McDonald, Graeme Plank, Beata Bukosa, Wayne Dillon, Jacques Pelon, Jean-Luc Baray, Frederic Tridon, Franck Donnadieu, Frédéric Szczap, Anja Engel, Paul J. DeMott, and Cliff S. Law

ABSTRACT: The goal of the Sea2Cloud project is to study the interplay between surface ocean biogeochemical and physical properties, fluxes to the atmosphere, and ultimately their impact on cloud formation under minimal direct anthropogenic influence. Here we present an interdisciplinary approach, combining atmospheric physics and chemistry with marine biogeochemistry, during a voyage between 41° and 47°S in March 2020. In parallel to ambient measurements of atmospheric composition and seawater biogeochemical properties, we describe semicontrolled experiments to characterize nascent sea spray properties and nucleation from gas-phase biogenic emissions. The experimental framework for studying the impact of the predicted evolution of ozone concentration in the Southern Hemisphere is also detailed. After describing the experimental strategy, we present the oceanic and meteorological context including provisional results on atmospheric thermodynamics, composition, and flux measurements. In situ measurements and flux studies were carried out on different biological communities by sampling surface seawater from subantarctic, subtropical, and frontal water masses. Air–Sea-Interface Tanks (ASIT) were used to quantify biogenic emissions of trace gases under realistic environmental conditions, with nucleation observed in association with biogenic seawater emissions. Sea spray continuously generated produced sea spray fluxes of 34% of organic matter by mass, of which 4% particles had fluorescent properties, and which size distribution resembled the one found in clean sectors of the Southern Ocean. The goal of Sea2Cloud is to generate realistic parameterizations of emission flux dependences of trace gases and nucleation precursors, sea spray, cloud condensation nuclei, and ice nuclei using seawater biogeochemistry, for implementation in regional atmospheric models.

KEYWORDS: Aerosol nucleation; Aerosol-cloud interaction; Air-sea interaction; Biosphere/atmosphere interactions; Primary aerosol; Secondary organic aerosol

https://doi.org/10.1175/BAMS-D-21-0063.1
Corresponding author: Karine Sellegri, k.sellegri@opgc.cnrs.fr
Supplemental material: https://doi.org/10.1175/BAMS-D-21-0063.2

In final form 30 August 2022

AFFILIATIONS: Sellegri, Peltola, Rocco, Freney, Rose, Bazantay, Planche, Banson, Joseph, Jourdan, Mioche, Colomb, Baray, Tridon, and Szczap—Université Clermont Auvergne, CNRS, Laboratoire de Météorologie Physique, Clermont-Ferrand, France; **Harvey*, Barr, Marriner, McGregor, Deppeler, and Bukosa**—National Institute of Water and Atmospheric Research, Wellington, New Zealand; **Saint-Macary, Cristi, and Law**—National Institute of Water and Atmospheric Research, Wellington, and Department of Marine Sciences, University of Otago, Dunedin, New Zealand; **Barthelmeß and Engel**—GEOMAR, Helmholtz Centre for Ocean Research Kiel, Kiel, Germany; **Moore and DeMott**—Department of Atmospheric Science, Colorado State University, Fort Collins, Colorado; **Peyrin and Donnadieu**—Université Clermont Auvergne, CNRS, OPGC, Clermont-Ferrand, France; **Labonnote**—Université Lille 1, Laboratoire d'Optique Atmosphérique, Lille, France; **Safi**—National Institute of Water and Atmospheric Research, Wellington, and Hamilton, New Zealand; **Archer**—Auckland University, Auckland, New Zealand; **Dunne and Harnwell**—Oceans and Atmosphere, CSIRO, Aspendale, Victoria, Australia; **Delanoe and Pelon**—Université Versailles Saint Quentin, CNRS, LATMOS, Versailles, France; **Saiz-Lopez, Quintanilla-López, and Lebrón-Aguilar**—Department of Atmospheric Chemistry and Climate, Institute of Physical Chemistry Rocasolano, CSIC, Madrid, Spain; **Rinaldi**—National research Council of Italy (CNR), Institute of Atmospheric Sciences and Climate (ISAC), Bologna, Italy; **Lupascu**—Institute for Advanced Sustainability Studies, Potsdam, Germany; **Olivares**—National Institute of Water and Atmospheric Research, Auckland, New Zealand; **Querel**—National Institute of Water and Atmospheric Research, Lauder, New Zealand; **McDonald and Plank**—University of Canterbury, Christchurch, New Zealand; **Dillon**—Department of Chemistry, University of Otago, Dunedin, New Zealand

* Deceased

This paper is dedicated to Mike Harvey, who played a leading role in the Sea2Cloud campaign and whose scientific contribution and collaboration in this and other research will be sadly missed.

Prediction of clouds over the Southern Ocean (SO) results in too much shortwave radiation reaching the ocean surface, inducing a large systematic bias that peaks during austral summer (Protat et al. 2017; Bodas-Salcedo et al. 2012). This is partly due to a lack of understanding of cloud formation and evolution in this poorly characterized part of the world. Aerosol–cloud interaction studies performed in the SO showed that stratocumulus cloud droplet size decreased to a greater degree with a fixed increase in aerosol particles during periods of higher ocean chlorophyll-a (Chl-a) (Sorooshian et al. 2009). Using SeaWiFS Chl-a Vallina et al. (2006) estimated that biogenic emissions in the SO account for 80% of the cloud condensation nuclei (CCN) column at 0.2% sursaturation during summer, whereas their contribution in winter was 35%. Gabric et al. (2002) showed correlations of satellite-derived Chl-a and aerosol optical depth (AOD) over the SO. These observations point to a significant impact of ocean biology on cloud-forming particles and subsequent cloud properties in this region. Yet the mechanisms by which ocean biology influences cloud properties are currently poorly constrained in climate and numerical weather predictions. Global models tend to underpredict the number concentration of marine aerosol, pointing to a missing particle source in the marine boundary layer (Hodshire et al. 2019; McCoy et al. 2020). Consequently, there is a need to better understand emission processes driven by biological mechanisms.

Marine microorganisms can influence cloud properties via two principal mechanisms: 1) emitting gas-phase components that form new particles via gas-to-particle conversion (or nucleation), and 2) influencing sea spray particles ejected to the atmosphere. The processes of nucleation and early growth lead to the occurrence of new particle formation (NPF) in the atmosphere, and, as these particles are numerous, they significantly affect the number of

global CCN (Merikanto et al. 2009). Yet, over the open oceans, particle formation events have only occasionally been observed in the marine boundary layer (MBL) (Clarke et al. 1998; O'Dowd et al. 2010; Baccarini et al. 2021), and so seem to be relatively rare. Several studies indicate that nucleation occurs in the marine free troposphere, where the condensation sink represented by sea spray and temperature are lower, and more light is available (Covert et al. 1992; Clarke and Kapustin 2002; Rose et al. 2015). Zheng et al. (2021) suggest that NPF may instead occur in the upper MBL, facilitated after precipitation following the passage of a cold front. Peltola et al. (2022) suggest nucleation actually occurs frequently in the marine boundary layer, contributing about 30% of sub-10-nm particle concentrations, and that this has been systematically overlooked due to the weak intensity and unconventional shape of these events.

Due to the difficulty in detecting NPF events in the MBL, the nature of the precursors to new particles remains an open question. Whereas reactive iodine species released by macroalgae are responsible for NPF events in coastal areas (O'Dowd et al. 2002a,b; McFiggans et al. 2004; Sellegri et al. 2005; Saiz-Lopez and Plane 2004; Saiz-Lopez et al. 2012; Sipilä et al. 2016), the link between phytoplankton and iodine emissions over the open ocean is still unclear, even though links between diatoms and halocarbons concentrations have been evidenced (Thorenz et al. 2014). Iodine and amines were both shown to play a role in new particle formation from marine biogenic emissions in a mesocosm study (Sellegri et al. 2016); however, dimethyl sulfide (DMS) is generally regarded as the main species driving secondary aerosol number production and CCN number (Charlson et al. 1987; Fitzgerald 1991; Ayers and Gras 1991) and is the only species implemented in global models (Boucher et al. 2003; Bopp et al. 2003; Korhonen et al. 2008). Yet field studies seeking a direct link between DMS emissions and CCN number have had variable success (Hegg et al. 1991; Andreae et al. 1995; O'Dowd et al. 1997; Tatzelt et al. 2022). NPF events do not necessarily occur even when the H_2SO_4 concentration is very high (10^8 cm^{-3}; Weber et al. 2001), and other CCN sources are required to explain observations (Sorooshian et al. 2009; Quinn and Bates 2011). New oxidation pathways of DMS and other organic sulfur species (Veres et al. 2020; Edtbauer et al. 2020) may lead to condensable species generating open ocean NPF that are currently not accounted for.

In addition, the relationship between biological activity and natural oxidants needs to be investigated using a statistically robust approach, in order to evaluate whether future modification will modulate atmospheric nucleation frequency and the rate of new particle growth. Among the oxidants responsible for the formation of low-volatility species potentially involved in new particle formation, ozone is particularly interesting for SO chemistry. Column ozone decreased drastically over 1960–90 in the 35°–60°S latitude range, in combination with greenhouse gas increases (Langematz 2018), whereas the increase in surface ozone observed in clean Southern Hemisphere air over the last 30 years is expected to continue (Cooper et al. 2020). This has led to an increase in oceanic iodine emissions over the mid-twentieth century (Cuevas et al. 2018; Legrand et al. 2018), due to deposition of ozone over the ocean and subsequent oxidation of dissolved iodide to produce hypoiodous acid (HOI) and molecular iodine (I_2), which then equilibrate with the atmosphere (Carpenter et al. 2013; MacDonald et al. 2014). Yet current model simulations indicate a negative feedback between surface ozone increase and ocean iodine, with ocean emissions buffering ozone pollution (Prados-Roman et al. 2015). Recent work in the Indian Ocean and SO has revealed that reactive atmospheric iodine is significantly correlated with Chl-a, indicating a biogenic control on iodine emissions (Inamdar et al. 2020). The magnitude and regional variability of abiotic versus biotic contributions to iodine emission from the ocean remains an open question.

At wind speeds greater than 4 m s^{-1}, breaking waves generate bubbles that burst into film, spume, and jet drops, and generate primary marine aerosol particles, or sea spray aerosol (SSA). Sea spray aerosol makes up 60%–85% of natural aerosol emissions, with an estimated contribution of 2,000–10,000 Tg yr^{-1} (Gantt and Meskhidze 2013; Seinfeld and Pandis 2006).

Discrepancies between modeled and observed number (Regayre et al. 2020) and mass (Bian et al. 2019) concentrations of marine aerosols point to a bias in the prediction of submicron sea spray. The chemical composition of sea spray contains both inorganic sea salt and organic material. Primary emissions can contain organic material as coated bubbles burst at the ocean's surface, in part derived from the organic-rich microlayer at the ocean surface (Bigg and Leck 2008; Lion and Leckie 1981). Marine organic aerosol particle mass is highly dependent on biological productivity in the surface ocean (O'Dowd et al. 2008; Sciare et al. 2009), and some mesoscale and global atmospheric models use Chl-a to predict sea spray organic fractions (Langmann et al. 2008; Vignati et al. 2010); however, the impact of seawater organic content on CCN number concentration differs in the literature. Estimates indicate the increase of sea spray mass due to organic enrichment accounts for <50% increase in CCN abundance (Burrows et al. 2022). Another potential pathway by which biology may influence sea spray–related CCN emissions is via organic matter alteration of the bubbling process and subsequent submicron sea spray number emission fluxes (Sellegri et al. 2021). Biological activity may also influence the temperature dependence of sea spray number fluxes, by changing the temperature dependence of seawater physical properties (Sellegri et al. 2022), which determines bubble films stability and lifetime, thereby explaining the large unexplained differences in temperature dependences reported in the literature (Salter et al. 2015; Schwier et al. 2017; Forestieri et al. 2018).

In addition, microbes (such as viruses and bacteria), detritus, exudates, and by-products in seawater may influence cloud properties via their ice nucleating properties. Indeed, a global modeling exercise suggested that marine bioaerosols may be the dominant source of ice nucleating particle (INP) number concentrations in the SO, and so influence the radiative and precipitation properties of clouds (Burrows et al. 2013). Wilson et al. (2015) and DeMott et al. (2016) suggested that marine biogenic sea spray are the primary source of INP in remote marine environments, particularly in the SO, and Vergara-Temprado et al. (2017) showed that accounting for the specificities of marine INP emissions gives better agreement between model simulations and observed cloud radiative properties for the remote SO. Recent observations have revealed that INP emissions are quite low over the SO (McCluskey et al. 2018a,b); however, there is a lack of observations to demonstrate their dependence on marine productivity (Welti et al. 2020). Glucose was pointed out as a potential tracer for phytoplankton-related ice nuclei activity in Arctic seawater (Zeppenfeld et al. 2019).

The sea surface microlayer (SML) is of particular importance to the sea-to-air exchange mechanisms and potential biological contribution described above. The SML is operationally defined as a layer with a depth of 0.001–1 mm (Hunter 1980), which is in direct contact with the atmosphere. The SML exhibits different properties to the underlying surface water (Cunliffe et al. 2013), with biological, chemical, and physical characteristics changing sharply below $60 \pm 10\ \mu$m (Zhang et al. 2003). The SML controls mass and energy flux to the atmosphere both directly and indirectly due to biological and chemical interference (Engel et al. 2017). Conceptually, the SML is viewed as a thin, dynamic, and gelatinous matrix composed of biogenic surface-active substances scavenged by rising bubbles (Cunliffe et al. 2013). The SML provides a habitat that is readily colonized by autotrophic and heterotrophic organisms (Sieburth 1983; Cunliffe and Murrell 2009). Unique dynamics influence SML properties; for example, gel aggregation from exopolymeric substances is increased by compression and dilation of capillary waves, with accumulation further enhanced by the natural buoyancy of gels (Wurl et al. 2011; Mari et al. 2017). The SML is often enriched with biogenic labile substances, such as amino acids (Kuznetsova and Lee 2001; Zäncker et al. 2017; Engel et al. 2018), and extreme solar radiation also influences organic matter cycling in the SML via abiotic photochemical alteration and also as a biotic stressor (Santos et al. 2012; Galgani and Engel. 2016; Miranda et al. 2018). Understanding these differing modes of organic matter production and enrichment in the SML is central to constraining air–sea exchange.

Objectives and general strategy

The main goal of the Sea2Cloud project was to investigate how the biogeochemical properties of surface seawater in the Southern Ocean impacts the fluxes and composition of volatile trace gases, aerosol particles [or condensation nuclei (CN)], CCN and INP of marine origin, and ultimately cloud properties (including cloud phase) (Fig. 1). The main research questions that guided the design of this study were as follows: 1) Does nucleation and early growth occur from marine emissions in the open ocean, and if so, from which chemical precursors? 2) Are these chemical precursors emitted by biotic or abiotic processes? If related to seawater microorganisms, can their fluxes be parameterized as a function of a biogenic tracer represented in remote sensing products and/or contemporary biogeochemical models? 3) How do emissions change in relation to variation in atmospheric ozone concentration? 4) How do biological properties of seawater interplay with physical seawater properties (such as temperature) to modulate sea spray fluxes? 5) To what extent does the biodiversity of oceanic surface water shape that of airborne microbial communities? 6) What are the INP fluxes to the atmosphere of marine origin, and do they correlate with a biological proxy represented in remote sensing products and models? And 7) how do CCN and INP fluxes of biological origin alter cloud properties above the Southern Ocean?

Previous scientific campaigns have been addressing some of the key questions stated above. Among the most recent, the Antarctic Circumnavigation Expedition: Study of Preindustrial-like Aerosol Climate Effects (ACE-SPACE) campaign focused on questions 1 and 8 via continuous measurements of aerosol and gas characteristics relevant for aerosol–cloud interactions around Antarctica and the Southern Ocean (Schmale et al. 2019). The goal of the Surface Ocean Aerosol Processes (SOAP), 2012, was characterizing the variation in aerosol composition and concomitant marine sources in the southwest Pacific (Law et al. 2017) to partly address questions 1 and 4. The project Marine biological production, organic aerosol Particles and marine Clouds (MarParCloud) had a focus on the organic content of ambient aerosol particles measured in the tropics, and their relation to the SML and also CCN and INP (van Pinxteren et al. 2020), and so contributed to questions 5, 7, and 8. The projects CAPRICORN, MICRE, MARCUS, and SOCRATES focused on aerosol–cloud interactions over the Southern Ocean, but did not include an ocean biogeochemistry component (McFarquhar et al. 2021). These studies all generated significant knowledge on how clouds are related to marine aerosol properties; however, biogenic fluxes were not measured directly, but were

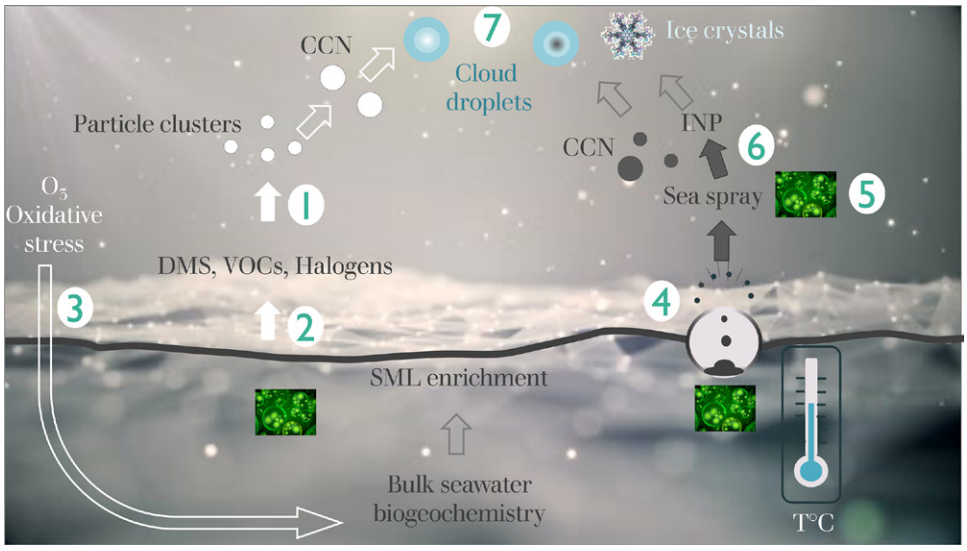

Fig. 1. Schematic of the general objectives and numbered scientific questions (see text) of the Sea2Cloud voyage, focused on parameterizing relationships (filled arrows) involving biological impacts.

instead based on ambient air measurements. As the latter reflect the integration of sea-to-air fluxes, chemical transformations and washout processes along the back trajectory, dilution in a changing marine boundary layer depth, and inputs from other atmospheric layers such as the free troposphere, it is difficult to establish a direct relationship between seawater biogeochemistry and aerosol emissions.

Investigating the relationships between ocean biogeochemistry and cloud precursors is especially relevant to the Southern Hemisphere due to its sensitivity to change in natural source emissions, due to low anthropogenic activities and the large impact of (white) clouds on the predominant dark ocean. Within the Southern Hemisphere, the Chatham Rise area, located east of New Zealand, was chosen as an ideal area for investigation. The Subtropical Front runs from west to east along the Chatham Rise at 43°–43.5°S, and separates the two major regional masses of subtropical and subantarctic water. Both water masses are relatively low in terms of productivity, whereas the frontal zone between them supports significant phytoplankton biomass. As a result, the Subtropical Front is characterized by elevated productivity year round, with large phytoplankton blooms evident in ocean color images (Murphy et al. 2001). Variable water mass mixing and eddy progression along the front results in blooms of different phytoplankton groups, including dinoflagellates, coccolithophores, and diatoms (Chang and Gall 1998; Delizo et al. 2007; Law et al. 2017). As these groups have different elemental and organic composition, and also nutrient requirements, they have contrasting influences on surface ocean biogeochemistry. This combination of contrasting water mass characteristics and high phytoplankton biomass and diversity makes this region an ideal laboratory for studying the influence of biogeochemical variability on aerosol composition and cloud dynamics (Law et al. 2017). Further regional benefits include exposure to relatively clean air from the SO, with only moderate terrestrial influence from the New Zealand mainland, and also wind speeds, wave height, and fetch that are representative of the SO (Smith et al. 2011).

The Sea2Cloud voyage took place on the R/V *Tangaroa* in this region in late austral summer (15–27 March 2020), as this season has been previously demonstrated to show significant range in productivity and phytoplankton type. The voyage strategy was based upon the successful approach utilized on the PreSOAP (2011) and SOAP (2012) voyages, which maximized sampling of water types and biogeochemistry while targeting phytoplankton blooms evident in satellite ocean color images (Law et al. 2017). Sea2Cloud backscatter images (b_bp443) (Fig. 2) enabled

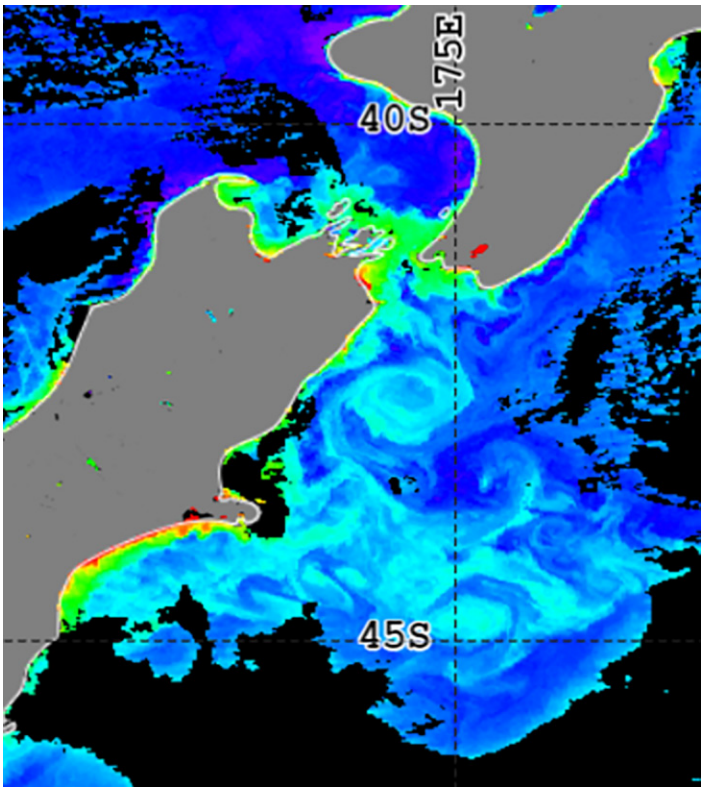

Fig. 2. Satellite image of ocean color (b_bp443) on 14 Mar 2020, highlighting the variability and structure of blooms along the Chatham Rise during the Sea2Cloud voyage. b_bp443 extends from 0.001 (purple) to 0.1 m^{-1} (red) with the elevated values on the western Chatham Rise along 44°S, 175°E reaching 0.05 m^{-1}. Image data generated by the Visible Infrared Imaging Radiometer Suite (VIIRS) on board the *Suomi National Polar-Orbiting Partnership* (*SNPP*) satellite; data courtesy of NOAA/NESDIS Center for Satellite Applications and Research.

regional location of different blooms, with continuous measurement of time surface water properties, including chlorophyll fluorescence and pCO_2, that enabled near-field location of phytoplankton blooms and position adjustment. In addition, the voyage track was determined by the need to maximize exposure to clean air, with a windward vessel heading maintained, particularly when winds were from the south.

It was essential, prior to the voyage design, to clearly identify how marine emissions would be implemented in the models. This approach required atmospheric and marine scientists to codesign joint experiments and exchange knowledge, both experimental and theoretical, for a better understanding of air–sea relationships. The voyage framework was therefore interdisciplinary, combining atmospheric physics and chemistry with marine biogeochemistry, and included ambient underway measurement of surface seawater and atmosphere, onboard experiments, and incubations. As atmospheric and ocean transport occur over different temporal and spatial scales, this prevents direct comparison of collocated measurements in the atmosphere and underlying ocean. Consequently, in addition to continuous ambient air measurements and 4-hourly sampling of surface water biogeochemistry, we also quantified physical and chemical fluxes as a function of biogeochemical properties in dedicated experiments. Other activities included sampling of the SML at distance from the R/V *Tangaroa* on a workboat, ocean CTD profiling of the upper 150 m, and atmospheric radiosonde deployment. The sampling and experimental layout of the vessel is summarized in Fig. 3, with each voyage component described below.

To simulate sea spray emissions that take place under high wind speeds, surface seawater was used in a plunging jet apparatus that mimics wave-breaking processes and artificially generates SSA (section S1.4). The procedure to derive fluxes as a function of air entrainment that can be used in modeling exercise can be found in Sellegri et al. (2021). Briefly, the surface water is exposed to air in a closed unit, with wave-breaking sea spray aerosol produced via a continuously circulating seawater jet system. The generated sea spray was characterized for full size distribution (5 nm–10 μm), 30-min-resolution chemical composition, daily size-segregated chemical composition, CCN and INP size-segregated concentrations, and biological content (Table ES4 in the online supplemental material; https://doi.org/10.1175/BAMS-D-21-0063.2). Despite the small size of the generator (10 L), the sea spray generated was shown to have a

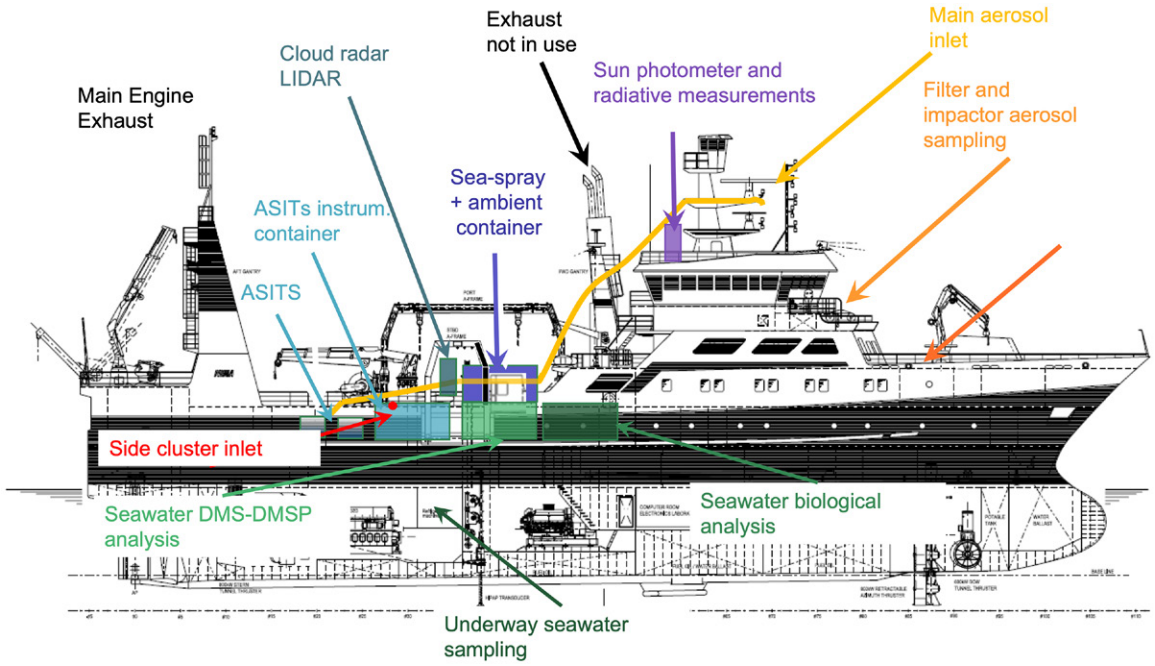

Fig. 3. General sampling and equipment layout on board R/V *Tangaroa* for the Sea2Cloud voyage.

stable size distribution across different campaigns (Schwier et al. 2015, 2017; Sellegri et al. 2021) that is consistent with other jet sea spray generators of comparable size and also size distributions generated by breaking waves (Sellegri et al. 2006; Fuentes et al. 2010). In the sea spray generator, the SML is considered to be reformed very rapidly (within 20 s; Kuznetsova and Lee 2001; Van Vleet and Williams 1983), with surface active material being adsorbed on the surface of rising bubbles and efficiently transported to the SML. Enrichment of organic matter and ice nucleating particles in the SML was also determined by sample collection at distance from the vessel using a workboat and dedicated SML sampling techniques (section S1.2). A novel addition to the sea spray generation experiments was investigation of the dependence of particle fluxes on seawater temperature in daily 1-h experiments, during which the temperature of seawater feeding the sea spray generation device was gradually decreased from 15° to 3°C (equivalent to the 25-yr average summer seawater temperature range of the SO; Auger et al. 2021).

Fluxes of gas-phase emissions and their potential to form new particles were evaluated within Air–Sea-Interface Tank (ASIT) experiments, in which the interaction of 1 m^3 of surface seawater with 1 m^3 of air headspace was characterized over ~2-day incubations (Fig. ES3). The goal of the ASIT experiments was to identify 1) the chemical nature of the precursors of nucleation and early growth of new aerosol clusters, 2) their dependence on headspace ozone concentration, 3) their link to seawater biogeochemistry, and 4) emissions of volatile organic compounds (VOC) and nanoparticle concentrations and composition. The headspace of the two ASITs was constantly flushed with aerosol-filtered air to evaluate the gas and aerosol fluxes at the sea–air interface (full experimental description is given in section S1.5) with the flushing rate and volume of the headspace resulting in a residence time on the order of 40 min. The two ASITs were covered with 8-mm-thick UV-transparent lids to allow natural light to enter and oxidize marine gaseous compounds within the headspace. A similar experimental setup proved to be effective for identifying and quantifying chemical species emitted from seawater that allowed nucleation and early growth to occur (Sellegri et al. 2016). While one of the ASITs was kept as a control (ASIT-control), the headspace of the other was enriched with ozone (ASIT-ozone) at an average of 8.5 ± 1.1 ppb relative to the ASIT-control, which is on the order of seasonal ozone variability and also the predicted long-term change in SO ozone concentration. A total of four ASIT experiments were performed with contrasted seawater types (Fig. 7), each lasting about two days. To generate parameterizations of aerosol nucleation rates as a function of identified gas phase precursors, the chemical composition at the molecular scale of newly formed clusters and their gas-phase precursors were determined. The analytical instrumentation included an atmospheric pressure interface–time of flight mass spectrometer (APi-ToF MS) (Junninen et al. 2010) and chemical ionization APi-ToF MS (CI-APi-Tof MS) (Jokinen et al. 2012), capable of elucidating nucleation mechanisms in simulation chambers (Kirkby et al. 2011; Kürten et al. 2014), but not previously applied in marine experimental incubations. Understanding of the chemical processes leading to the observed condensing species requires the measurements of parent chemical species, which were measured using a proton transfer reaction and mass spectrometer (PTR-MS) (Lindinger et al. 1998; Blake et al. 2009; Wang et al. 2012). In parallel, we determined the seawater biogeochemistry (section S1.5) for macronutrients, particulate carbon and nitrogen, dissolved organic carbon (DOC) composition including amino acids, fatty acids, colored and fluorescent dissolved organic matter (CDOM and fDOM, respectively), and phytoplankton biomass (Chl-a), abundance and speciation. Analysis of DMS, dimethylsulfoniopropionate (DMSP), and iodide concentration in the seawater was also performed. Due to the potentially important role in driving sea–air fluxes, SML samples were collected from the ASITs at the end of each experiment and analyzed

for biogeochemical properties (section S1.5). In addition, six deployments of the workboat enabled characterization of the SML and the underlying subsurface water (SSW; ~50 cm depth) in situ for the same parameters as in the ASITs, with the goal of relating the SML organic enrichment and volatile gases to the surface ocean biology.

Complementary models will be used to assess the impact of biological activity on aerosol, CCN, and INP fluxes. The flux parameterizations derived from the nascent sea spray and ASITs experiments will be implemented in the WRF-Chem model (Grell et al. 2005; Fast et al. 2006), and the resulting aerosol distributions in the model will be tested against in situ ambient measurements. Ambient measurements were performed using in situ Table ES1.1) and remote sensing instrumentation (Table ES6). Ambient atmospheric measurements comprise gas-phase concentrations (SO_2, ozone, VOCs), aerosol size distribution ranging from the nanoscale particle clusters (from 1 nm) to the supermicron mode, aerosol size-segregated chemical composition and metagenomic content, and aerosol CCN and INP properties. The approach taken to minimize local ship contamination and filter out contamination is described in sections S1.1.1 and S1.1.2. Remote sensing instrumentation enabled characterization of column-integrated gas-phase IO and BrO and aerosol size distribution, as well as the vertical profile of aerosol loading. The ultimate goal of the project, to assess the impact of marine biology on cloud properties, will be achieved using the detailed (bin) microphysics DESCAM scheme (Flossmann and Wobrock 2010; Planche et al. 2010, 2014). The aerosol fields generated from WRF-Chem will serve to initiate DESCAM in order to understand the impacts of aerosols on cloud properties, and in particular on the phase partitioning between cloud liquid- and ice-water phases (Bodas-Salcedo et al. 2019, among others). The DESCAM model cloud outputs will be tested against remote sensing data. Available remote sensing data for cloud characterization include the vertical profiles of cloud liquid and ice content, obtained by a combination of radar and lidar measurements. Rain and drizzle profiles were also measured for testing the ability of the model to predict the initiation of precipitation.

General seawater and atmospheric features

Meteorological context. Synoptic meteorology during the voyage was driven by an alternating sequence of low and high pressure and frontal systems with an approximate 4-day cycle duration (i.e., 2 days between pressure minima and maxima). Early in the voyage (15 March) meteorology was marked by the passage of a cold front followed by anticyclonic conditions, with a second cold front and low pressure system passing to the south on 19 March. From 20 to 21 March, high clouds slowly built and the cloud base steadily fell from ~8 km to the top of the marine boundary layer over 24 h with an approaching warm front. At 0900 UTC 21 March, the first and heaviest rain of the voyage fell (Fig. 4). Pressure then decreased as the vessel headed north, with lighter rain events accompanying the passage of several troughs in a moist westerly airstream to the end of the voyage on 27 March. Air temperature ranged between 8.4° and 20.1°C (average 13.1° ± 1.7°C) and wind speeds representative of the location/season, with a median of 10 m s^{-1} and reaching 26 m s^{-1} during the storm that occurred on 23 March.

Alternating pressure systems and west–east pressure difference across the South Island influences the northerly/southerly airflow to the east of the South Island as discussed by Peltola et al. (2022).

Airmass back-trajectories were calculated using the HYSPLIT model (Rolph et al. 2017; www.ready.noaa.gov/HYSPLIT_traj.php) with GFS meteorology at resolution 0.25° over the 72 h preceding the ship position. As shown in Fig. 5, air masses of contrasting origin were sampled during the voyage. The cleanest air masses with least terrestrial contact at the vessel were

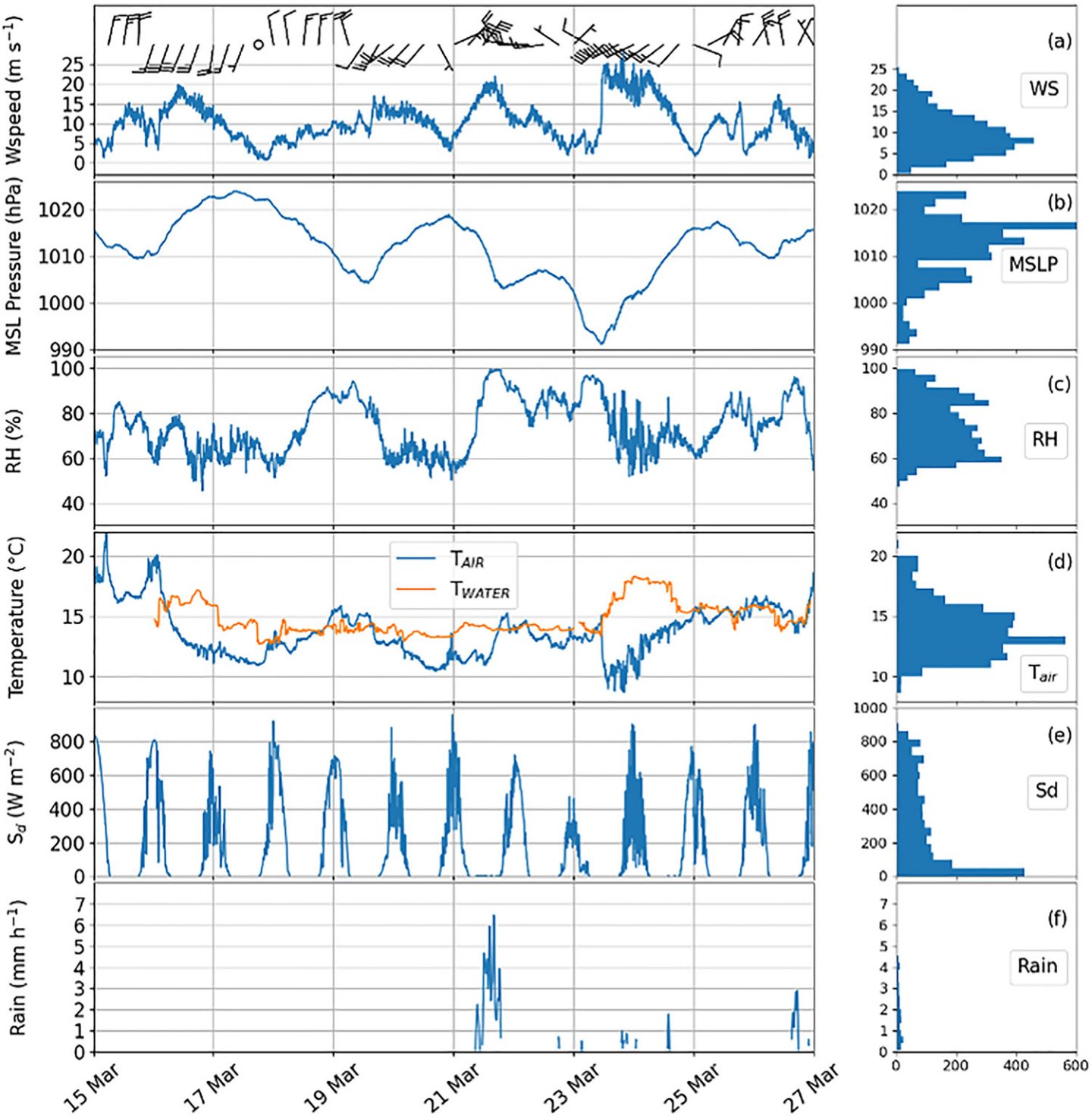

Fig. 4. Time series (UTC) and frequency distributions of (a) wind speed and direction barbs (full barb = 10 kt; 1 kt ≈ 0.51 m s^{-1}), (b) sea level pressure, (c) relative humidity, (d) air and sea surface temperatures, (e) downwelling shortwave radiation (S_d), and (f) rainfall rate.

southerly air from the bottom of the South Island (Figs. 5a,d,f,h), as opposed to northerly and frontal air masses (Figs. 5b,e,g,i,j) that were often influenced by air crossing the landmass of New Zealand. From the HYSPLIT back-trajectories, we also calculated the fraction of time spent over the ocean, within the MBL (altitude < 500 m) or in the marine free troposphere (MFT; altitude > 500 m) (Bigg et al. 1984), and over land in the planetary boundary layer (PBL; altitude < 1500 m) or in the planetary free troposphere (PFT) (Hara et al. 2021). Results are shown in Fig. 6, in which periods of clean SO air masses were sampled on

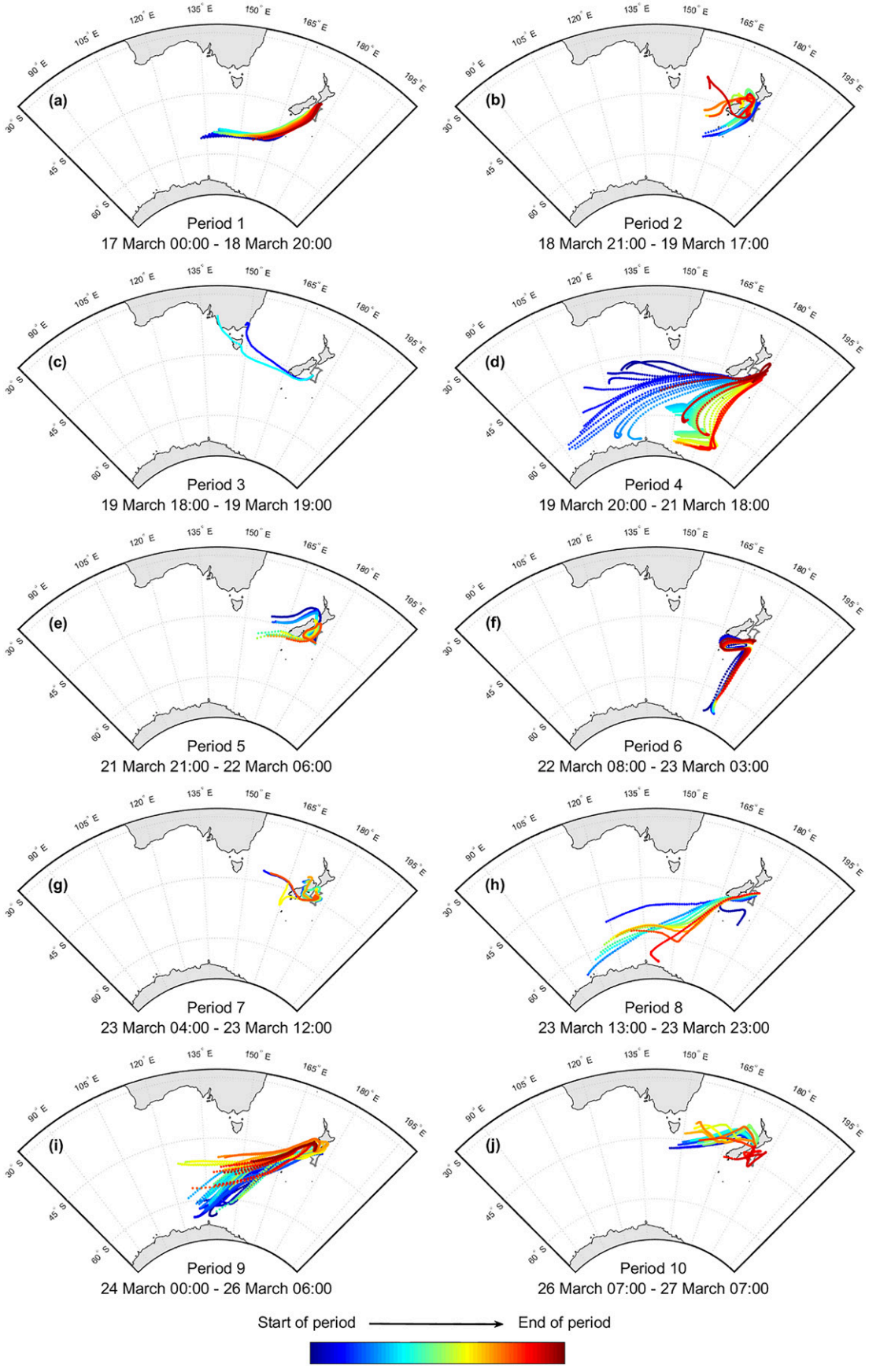

Fig. 5. Airmass back-trajectories calculated using the HYSPLIT model over the 72 h preceding the ship position. Periods characterized by air masses of contrasting origin have been identified throughout the campaign and are represented separately. The color code gives an indication of the sampling order of the different air masses within a period, and the ship's path is in addition shown in gray in each panel. Time is given in UTC.

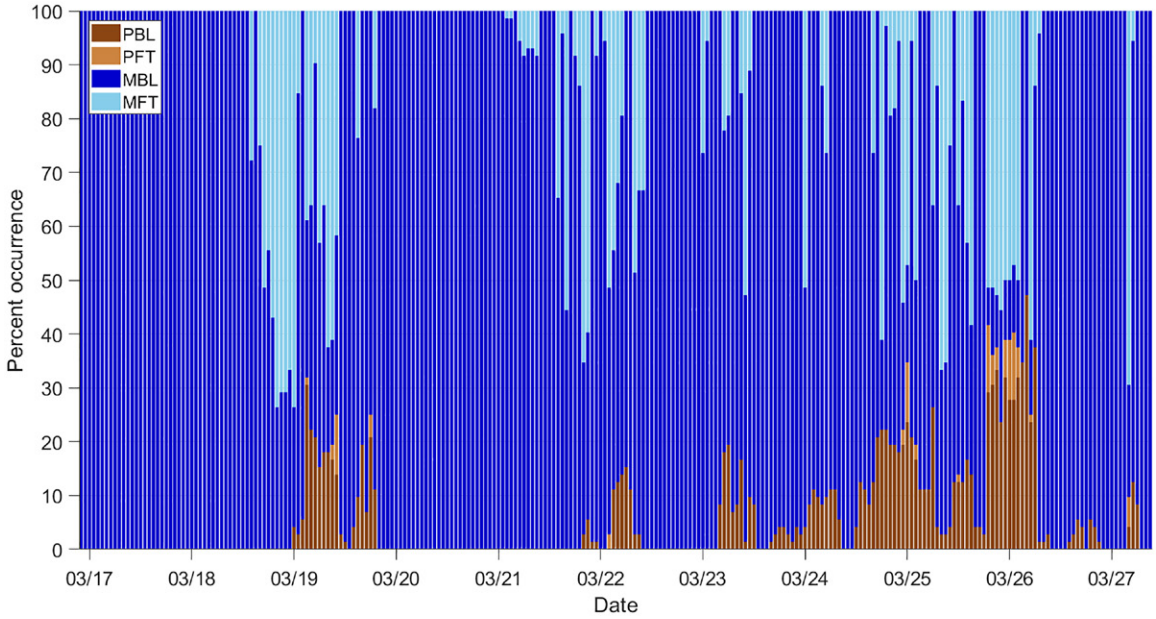

Fig. 6. Fraction of time for air spent in the MBL, MFT, PBL, and PFT as a function of time (UTC). See text for definition of abbreviations.

17 and 18 March (also see Fig. 5a), with occurrence of MFT air masses, and on 20, 21, and 22 March (also see Figs. 5d,f). This shows that air masses primarily traveled over the ocean in the free troposphere when a fraction of the air mass had been over land, indicating an uplifting effect of lands via forced convection, especially when air masses crossed the mountainous South Island. Consequently, the terrestrial influence on new particle formation events may be regarded as a potential source of chemical species, but also as a source of dynamical uplifting.

Seawater general properties. The vessel initially headed south from Wellington on 16 March (NZDT, local time) in order to sample elevated chlorophyll at the western end of the Chatham Rise at 43°25′S and clean southerly air masses. Chl-a (measured as described Table ES2 and section S2.1.1) was moderately high on the initial southerly transit, with an average 1.2 ± 0.35 mg m^{-3} over the first 12 h (Fig. 7c). After crossing the Chatham Rise the vessel sampled an area of elevated biomass (Chl-a: 2–3 mg m^{-3}) at 44°26′S, 174°E before heading east through frontal waters of variable Chl-a (point 1). A significant phytoplankton bloom was encountered at 44°44′S, 175°20′E on 19–20 March, with Chl-a values exceeding 3.5 mg m^{-3} (point 2). After sampling this bloom the vessel headed south, sampling intermediate biomass waters (0.5–1.2 mg m^{-3} Chl-a) at 45°50′S, 175°10′E on 20 March, and then east across low biomass subantarctic waters (1.30 ± 0.44 μg L^{-1}) (point 3). The passage of a warm front with heavy rainfall, during the overnight transect on 21 June, resulted in unusual traces of black carbon on seawater filters. The ship carried out local surveys in the vicinity of this rain event before heading north-northwest on 23 March. The vessel crossed the eastern end of the Chatham Rise on 24 March (point 4), and continued north-northeast during a strong southerly storm. Subtropical waters were subsequently sampled at 42°24′S, 175°35′E on 25 March (point 5), after which "mixed" water, influenced by flow through the Cook Strait, was sampled at 42°45′S, 175°35′E on 25 March (point 6). The subsequent plan to further sample the productive waters along the Subtropical Front was subverted by the return to Wellington on 26 March due to New Zealand COVID-19 restrictions. Sea surface temperature (SST) showed a 6.5°C range (12.8°–18.3°C) during the voyage, with a latitudinal trend of lowest temperatures during the southern transect

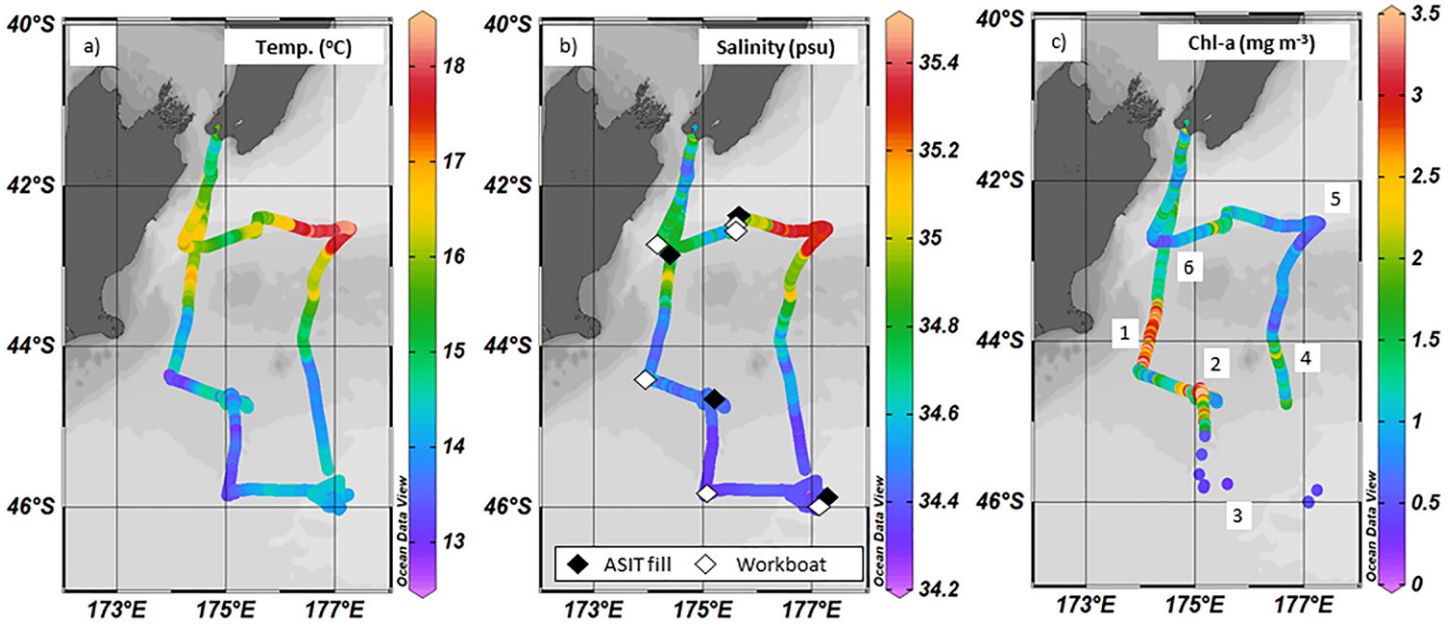

Fig. 7. (a) SST (°C), (b) salinity (psu), and (c) surface Chl-a (mg m^{-3}) along the Sea2Cloud voyage track shown against latitude (*y* axis) and longitude (*x* axis). In (b) the black diamonds indicate the location of seawater collection for the four ASIT experiments, and the white diamonds indicate the location of the six workboat deployments for SML sampling. In (c) surface chlorophyll fluorescence was measured continuously using an Ecotriplet sensor, except in the southeast corner of the track where discrete Chl-a results are shown instead. The letters in (c) correspond to events identified in the text above. The gray background shading indicates the bathymetry. Figure plotted using ODV (Schlitzer 2020).

and warmest in the northern transect. The salinity varied along the transect, and was used as an indicator of water type based upon previously identified thresholds (Chiswell et al. 2015) (Figs. 7b and 8).

Preliminary results

Underway seawater biogeochemistry. Figure 9a shows the variability of surface Chl-a during the voyage in relation to water mass type. This variability corresponded to sharp discontinuities in nutrient distribution, as indicated for nitrate concentration in Fig. 9b, with coincident variability in frontal waters, and also the high nitrate of the high-nutrient, low-chlorophyll (HNLC) subantarctic waters. Subtropical waters were low in nitrate

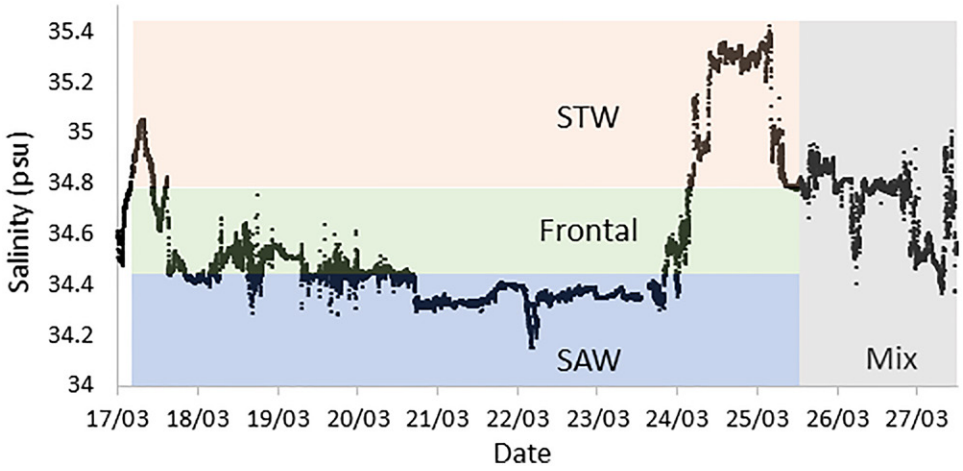

Fig. 8. Surface salinity, which was used to distinguish the different water types during the Sea2Cloud voyage. Subtropical water (STW) is defined by salinity > 34.8, frontal waters by salinity = 34.5–34.8, and subantarctic waters (SAW) by salinity < 34.5 (from Chiswell et al. 2015), with the date on the horizontal axis indicating the midday time point in NZDT.

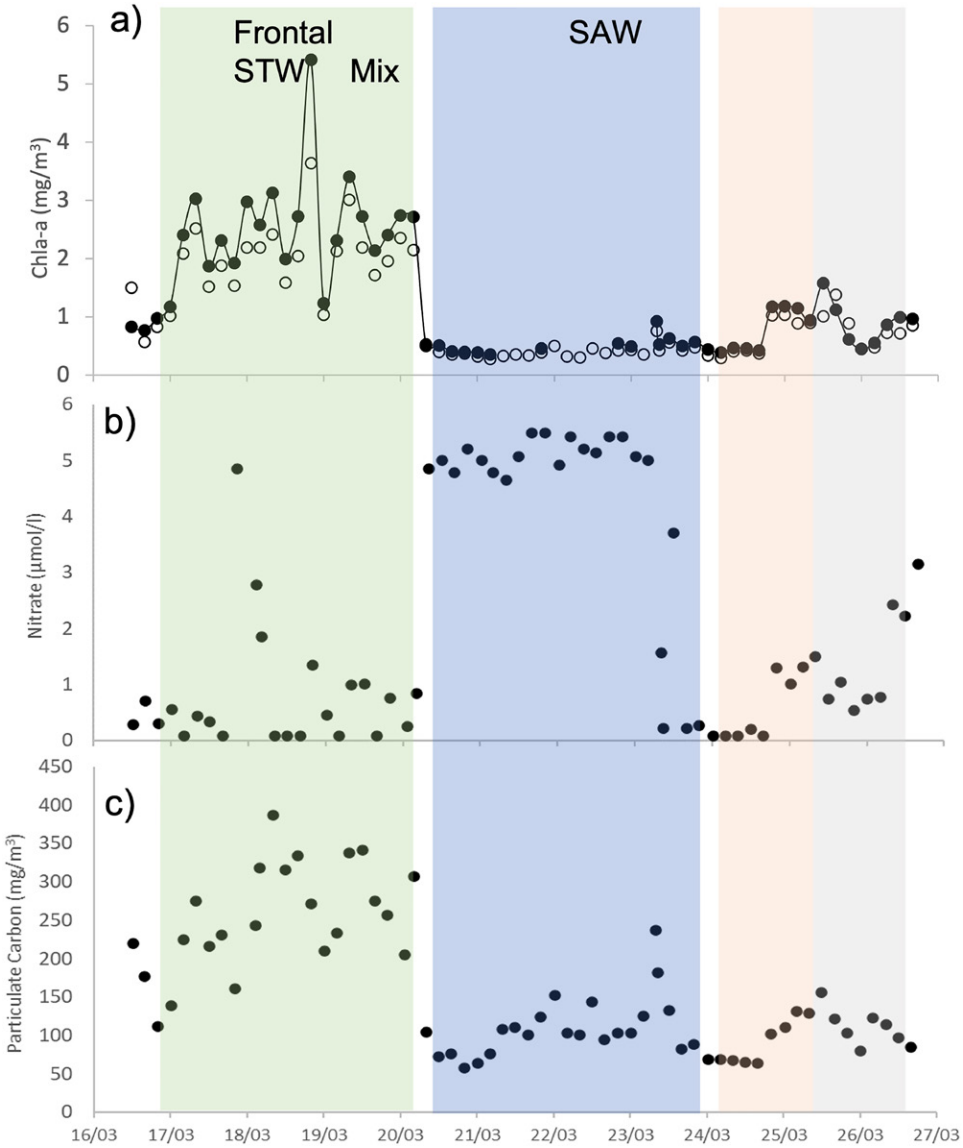

Fig. 9. Surface water concentrations of (a) chlorophyll-a (black circles: total Chl-a; white circles: total of all Chl-a size fractions), (b) nitrate, and (c) particulate carbon, with water mass type (designated by salinity) differentiated by the shaded columns, and date on the horizontal axis indicating midday in NZDT.

and phosphate, whereas silicate concentration showed the reverse, with lowest values (~0.5 μmol L^{-1}) in subantarctic water and highest values (~1.5 μmol L^{-1}) north of the Chatham Rise (data not shown). Particulate carbon reflected Chl-a concentration with elevated values in the bloom, minimum values in subantarctic waters, and sharp discontinuities between water masses.

Figure 10 shows the abundance of the major phytoplankton groups (dinoflagellates, diatoms, and flagellates; all >5 μm size), and also the biovolume in the micro- and nanophytoplankton size groups (>20 and 5–20 μm, respectively) in surface seawater throughout the voyage. Diatom abundance was highest in the frontal waters, whereas flagellates dominated the >5 μm phytoplankton community in the other water masses. Dinoflagellate abundance was low in all regions but contributed the most in subantarctic and subtropical waters. The bloom on 19 March was dominated by diatoms, with a high proportion of large (>20 μm) *Thalassiosira* sp. The biovolume of nanophytoplankton was generally equal to microphytoplankton in frontal and mixed waters, whereas it was larger than microphytoplankton in subantarctic and subtropical waters, as illustrated in Fig. 10b.

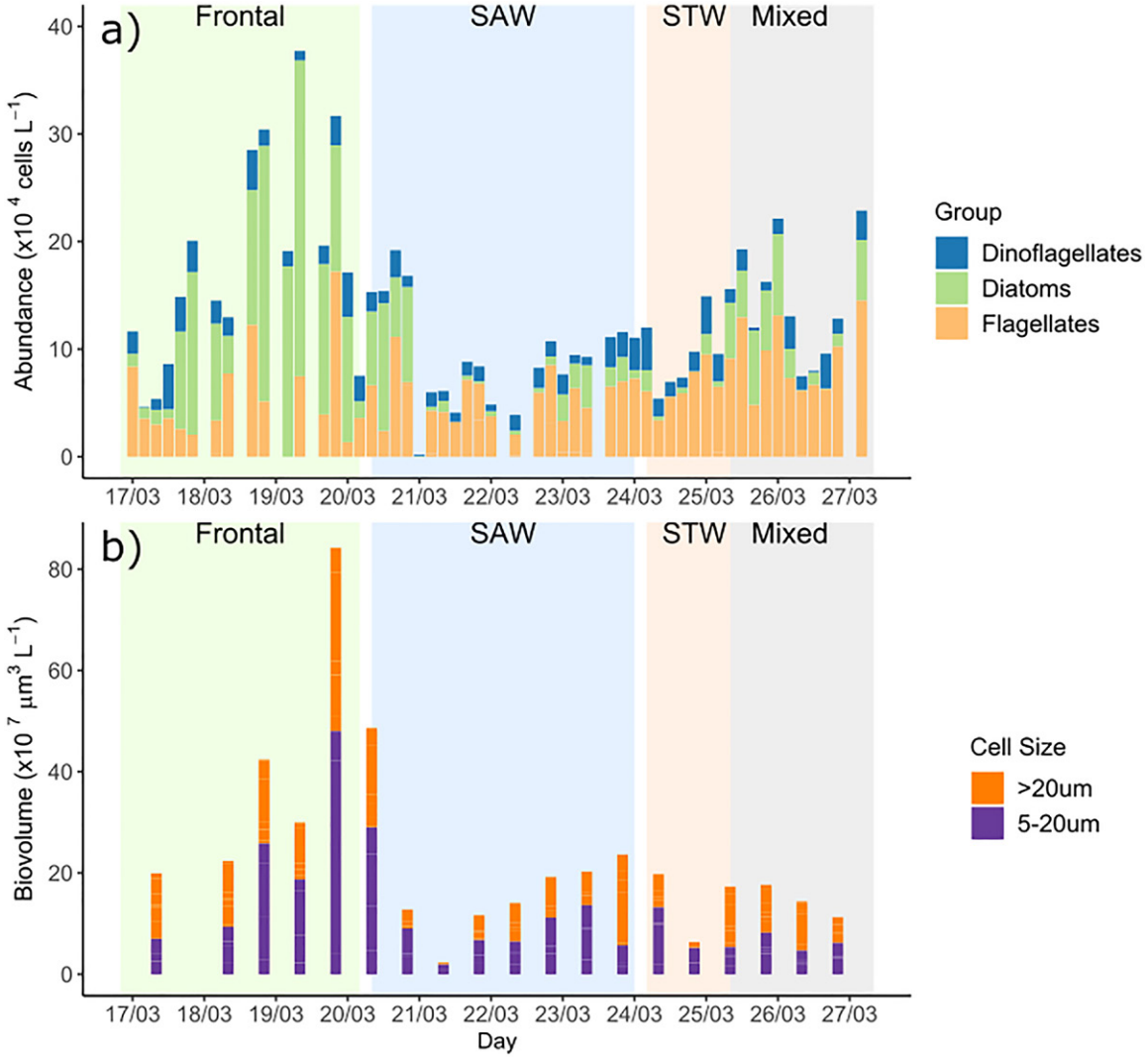

Fig. 10. (a) Abundance of the major phytoplankton groups, dinoflagellates (blue), diatoms (green), and small flagellates (orange), at 4-h intervals and (b) size distribution of phytoplankton (cell biovolume) at 0800 and 2000 NZDT each day, with water mass type (designated by salinity) differentiated by the shaded columns, with the date on the horizontal axis indicating the midnight time point in NZDT.

Cell abundance of picoeukaryotes (<2 μm) and *Synechococcus* generally showed an inverse relationship to the larger phytoplankton cell size groups, with a minimum in the bloom and frontal zone, and maxima in the subantarctic and subtropical water (data not shown).

Artificially generated nascent sea spray. In Sellegri et al. (2021), and also the Sea2Cloud dataset (Sellegri et al. 2022), the nanophytoplankton cell abundance was found to be related to the sea spray number flux while Chl-a showed no significant relationship. As stated in Sellegri et al. (2021), the hypothesis behind this relationship is that the nanophytoplankton is a major contributor of organic chemicals with surfactant properties that modify bubble lifetime when they reach the ocean surface, and so alter bubble film properties when they burst, so influencing the sea spray number emitted to the atmosphere. The median nascent sea spray size distribution can be decomposed into a nucleation mode at 12 nm, an Aitken mode at 38 nm, two accumulation modes at 108 and 290 nm, and a coarse mode at 1 μm (Fig. 11). This median sea spray size distribution is very similar to the one obtained with a similar sea spray generation system using Mediterranean surface seawater (~35°–45°N) during the PEACETIME campaign (Sellegri et al. 2021). The shape of the size distribution was

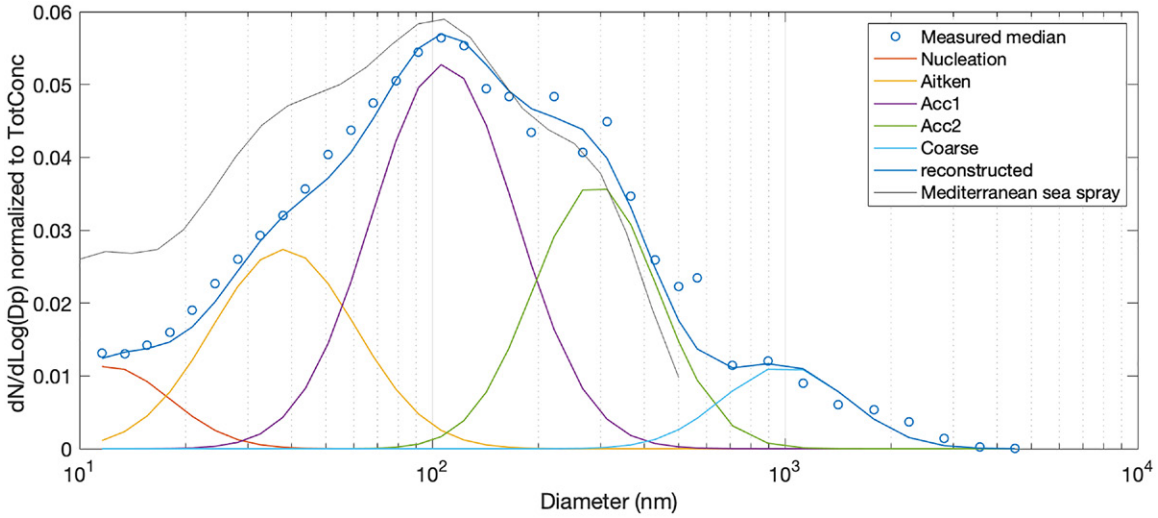

Fig. 11. Median nascent sea spray size distribution measured with DMPS and WIBS (see methods), normalized with the median total sea spray concentration, and decomposed into four submicron modes and one supermicron mode. In addition, data are compared to the average normalized sea spray size distribution measured from Mediterranean seawater with the same sea spray generation system as reported by Sellegri et al. (2021).

very stable across the Sea2Cloud voyage especially in the accumulation and coarse modes, and the ratio of the coarse mode particles (0.7–4 μm) to the accumulation mode particles (70–145 nm) was 0.27 by number and 3.6 by surface.

The organic and inorganic chemical components of SSA were measured offline on PM_1 filters, and online using a time of flight aerosol chemical speciation monitor (ToF-ACSM). The ToF-ACSM is configured to measure nonrefractory species with diameters less than 1 micron (PM_1). However, a number of recent studies (Ovadnevaite et al. 2017; Freney et al. 2021), have illustrated that under specific sampling conditions this instrument is capable of characterizing the total PM_1 SSA. This is confirmed through comparison with collocated number size distribution measurements, showing a relation of $r = 0.65$, $b = 0.67$ (Fig. ES7). The measured concentration was composed of almost 50% salt, and a variable organic fraction from 25% to 45%, with average contributions of 36% (Fig. 12a). This fraction, confirmed by offline filter measurements, is considerably higher than previous work in the Mediterranean where <10% of the PM_1 mass concentration was organic, but only 50% higher than reported in previous regional measurements of primary marine organics, which contributed up to 23% of the submicron SSA (Cravigan et al. 2020; Kawana et al. 2021). Positive matrix factorization analysis of this organic component resolved three main groups of organic species: an oxidized organic aerosol contributing to 40% of the organic mass, with the remaining 60% composed of primary organic aerosol, with similar signatures as those observed in the Mediterranean, and a less oxidized organic species containing signatures of methanesulfonic acid.

The fluorescent properties of aerosol particles larger than 500 nm in diameter were measured using a Wideband Integrated Bioaerosol Sensor (WIBS). Although a number of studies have described the fluorescence properties of ambient marine aerosols in the SO pristine environment (Moallemi et al. 2021; Kawana et al. 2021), this is, to our knowledge, the first time fluorescent properties of primary sea spray have been measured to infer the presence of biological material in nascent marine aerosol. During the sampling period, an average of 4% ± 4% of the particles fluoresced after excitation at wavelengths of 280 and 370 nm. This is considerably higher than fluorescent fractions observed in ambient

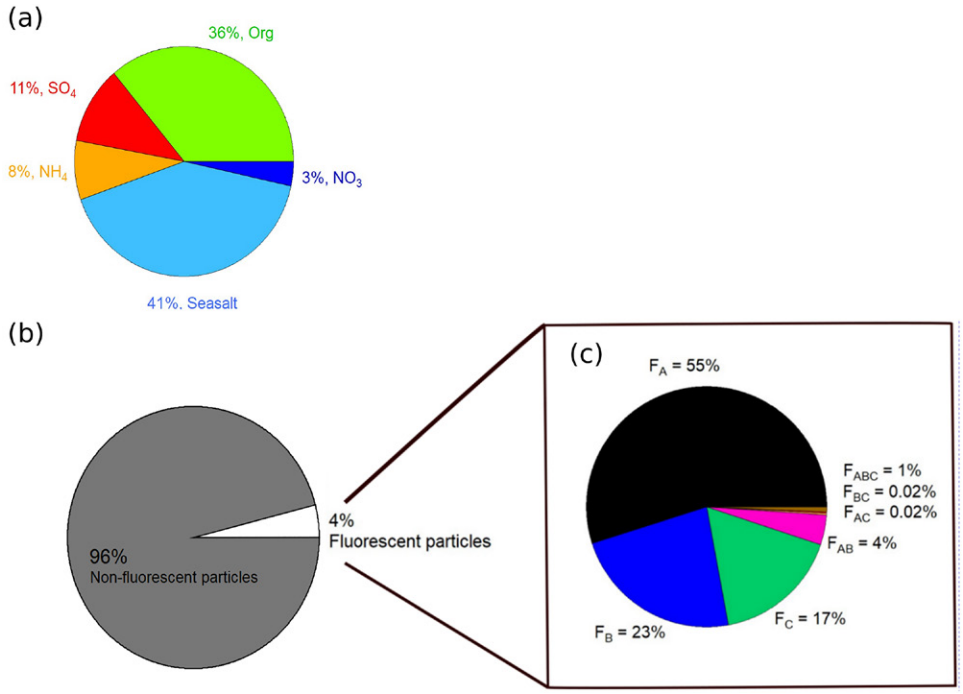

Fig. 12. (a) Fractional contribution of the different chemical species in the PM_1 aerosol, measured by the ToF-ACSM, (b) fraction of particles having fluorescent properties, and (c) the classification of the contribution (F) of each of the fluorescent types of aerosols > 500 nm [A (often related to bacteria), B (carbonaceous species), C (carbonaceous species], AB, AC, BC, ABC (combined channels are often indicative of supermicronic fluorescent material) averaged over the Sea2Cloud field campaign.

aerosol samples over the SO under pristine marine conditions (1.6%) and terrestrially influenced samples (2.2%) (Moallemi et al. 2021; Kawana et al. 2021). Using the classification published by Perring et al. (2015) and subsequently used in several studies, fluorescent particles are divided into seven different classes (A, B, C, AB, AC, BC, ABC, see Fig. 12b). In a laboratory environment, fluorescent particles classified as "A" (excited at 280 nm and emitting at 310–400 nm) have been associated previously with bacteria, while B (excited at 280 nm and emitting at 420–650 nm), and C (excited at 370 nm and emitting at 420–650 nm) are associated with carbonaceous species (Savage et al. 2017). As shown in Fig. 12c, the fluorescent fraction of sea spray was dominated by type A aerosol, likely bacteria, followed by carbonaceous species (B, C).

Nucleation from marine biogenic precursors. In each of the ASIT experiments the seawater biogeochemistry was characterized continuously by a submerged Exosonde sensor for temperature, salinity, dissolved oxygen, Chl-a fluorescence, and fDOM. In addition, three discrete seawater samples were collected at the beginning, middle and end of each 2-day experiment (see supplemental information for parameters). Sampling confirmed that the seawater composition reflected that of the different water masses sampled, with distinct differences in phytoplankton communities between experiments. In addition, there were some differences in seawater biogeochemical composition between the ASIT-control and ASIT-ozone at the end of each experiment, suggesting an influence of ozone addition (Rocco et al. 2023).

Figure 13 shows the time evolution of the number concentration of aerosol particles in the 1–2.5 nm size range during ASIT experiment with frontal seawater. This is the smallest detectable size range that contains freshly nucleated particles. While the concentrations stay typically below 10^{-2} cm^{-3} with a median of 2×10^{-3} cm^{-3} in the ambient bypass air, the concentrations in

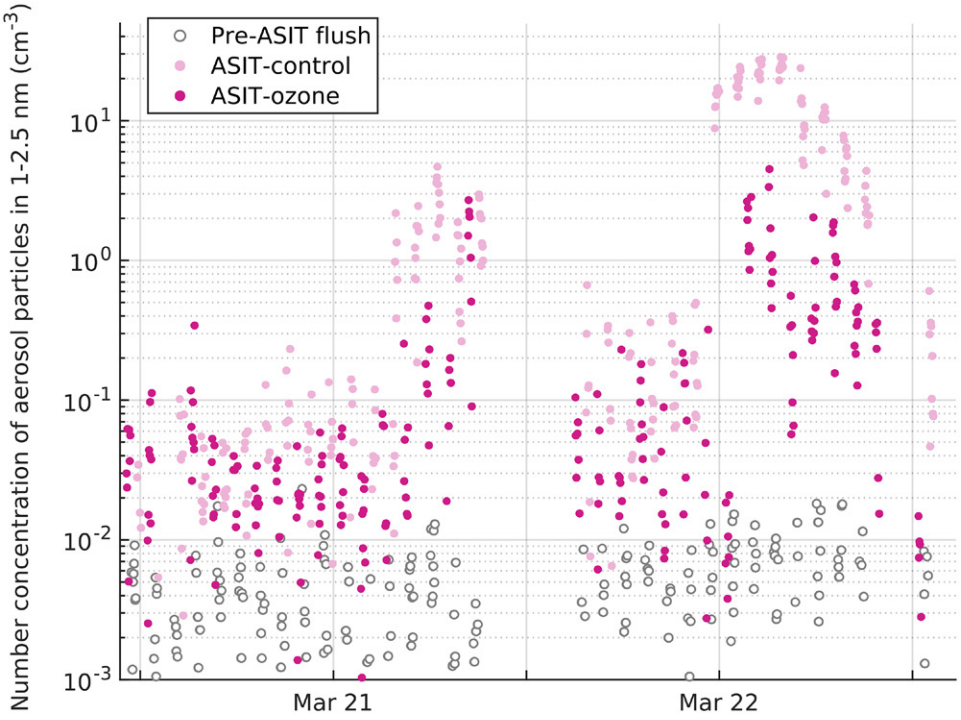

Fig. 13. Time evolution of number concentration of particles in 1–2.5 nm during the experiment with frontal bloom seawater. Ozone concentration in the ASIT-control was 6.6 ± 1.4 ppb while it was 14.8 ± 1.8 ppb in the ASIt-ozone.

the ASITs vary from below 0.01 to >10 cm^{-3} with medians of 0.3 and 0.1 cm^{-3} for ASIT-control and ASIT-ozone, respectively. The enhanced concentrations of these nascent ultrafine particles in the ASITs indicates that new particle formation was occurring in the headspace. However, the concentrations are relatively low, which is partially due to the low residence time of air in the tanks but also to the low-nucleation precursors in the clean open-ocean environment of the Southern Hemisphere. The combination of cluster-sized particle fluxes calculated from these concentrations, with those of potential precursor gases, among which were deriving from unexpected biogenic marine VOC fluxes (Rocco et al. 2021), will be used to determine quantitative parameterizations of short-term nucleation rates in the open-ocean boundary layer. The ASIT experiment also allowed to successfully relate these VOC fluxes to seawater phytoplankton cell abundances (Rocco et al. 2021, 2023).

Ambient aerosol and clouds. Figure 14 shows a map of particle number concentrations (Dp > 7 nm, CN_7), filtered from ship emission events (see online supplemental material). Mean CN_7 over the campaign was 1,133 ± 1,007 cm^{-3} (median: 774 cm^{-3})

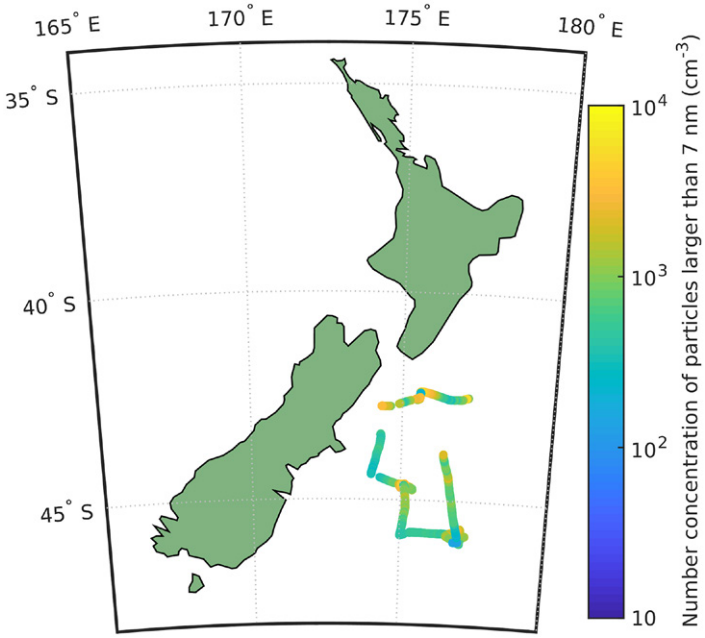

Fig. 14. Aerosol total concentrations from CPC over the ship's track.

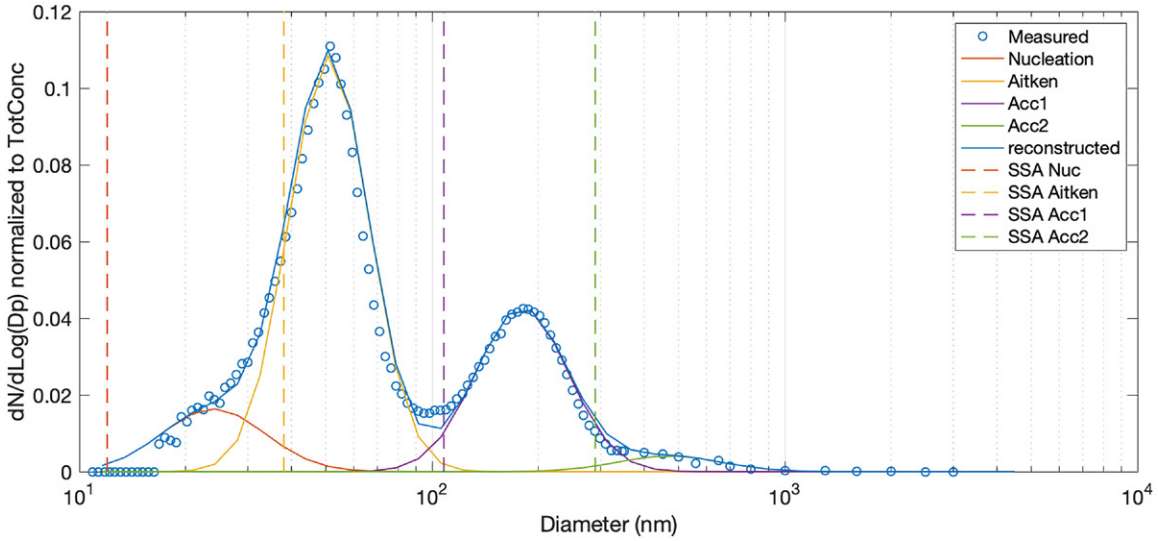

Fig. 15. Median aerosol size distribution measured from SMPS and OPC in ambient air during the first clean Southern Ocean sector period (17–18 March) defined by the HYSPLIT analysis, normalized with the median total sea spray concentration, and decomposed in four submicron modes. Dashed lines indicate where the SSA modes were found using the sea spray generator (shown Fig. 11).

overall and 711 ± 458 cm^{-3} (median: 541 cm^{-3}) in the clean marine air masses as described in the "Meteorological context" section (periods 1, 4, 6, 8). These results are similar to those reported from the SOAP voyage in the same region, with concentrations of 1,122 ± 1,482 cm^{-3} in terrestrially influenced air masses and 534 ± 338 cm^{-3} in clean marine air (Law et al. 2017), and also with a recent dataset from west of New Zealand with median CN_{10} of 681 cm^{-3} between 40° and 45°S and 350 cm^{-3} between 45° and 65°S (Humphries et al. 2021).

The median aerosol size distribution observed during 17–18 March when SO air masses prevailed at moderate wind speed showed a trimodal distribution with a dominating Aitken mode (geometric mean dry diameter at 50 nm), followed by two accumulation modes at 180 and 470 nm (Fig. 15). A contribution from nucleation mode particles at 24 nm was also found, indicating either the occurrence of NPF in clean marine boundary layer air masses, or the contribution of ultrafine sea spray particles (see "Artificially generated nascent sea spray" section). Overall, all modes contributing to ambient aerosol in clean SO air masses were measured at larger sizes than in nascent sea spray (in comparison to Fig. 11). The Aitken and first accumulation modes were more separated in the ambient air compared to nascent sea spray, and the Aitken mode dominated over the first accumulation mode in contrast to the nascent sea spray data. These two differences, in combination with the lower contribution of particles > 100 nm in ambient air relative to nascent sea spray, could be, among other factors, the result of cloud processing and aerosol wash out in ambient air, creating a clear Hoppel minimum and lower concentration of larger particles (especially the supermicron fraction).

Low-level (<2,000 m) and lower-midlevel clouds (2,000–3,000 m cloud top) occurred during a large fraction of the voyage, and in clean SO airmass periods, providing particularly favorable opportunities to study the link between ocean emissions and cloud properties. On 20 March, some low-level clouds contained a fraction of ice (Fig. 16b), and precipitation occurred (Fig. 16d). These data provide an opportunity to investigate the potential role of ice in the initiation of precipitation, and hence the role of ice nuclei of marine origin on the persistence of low-level clouds. The use of ambient seawater, aerosol and cloud measurements to ultimately link cloud properties to marine emissions will be tested using two approaches presented in the following sections.

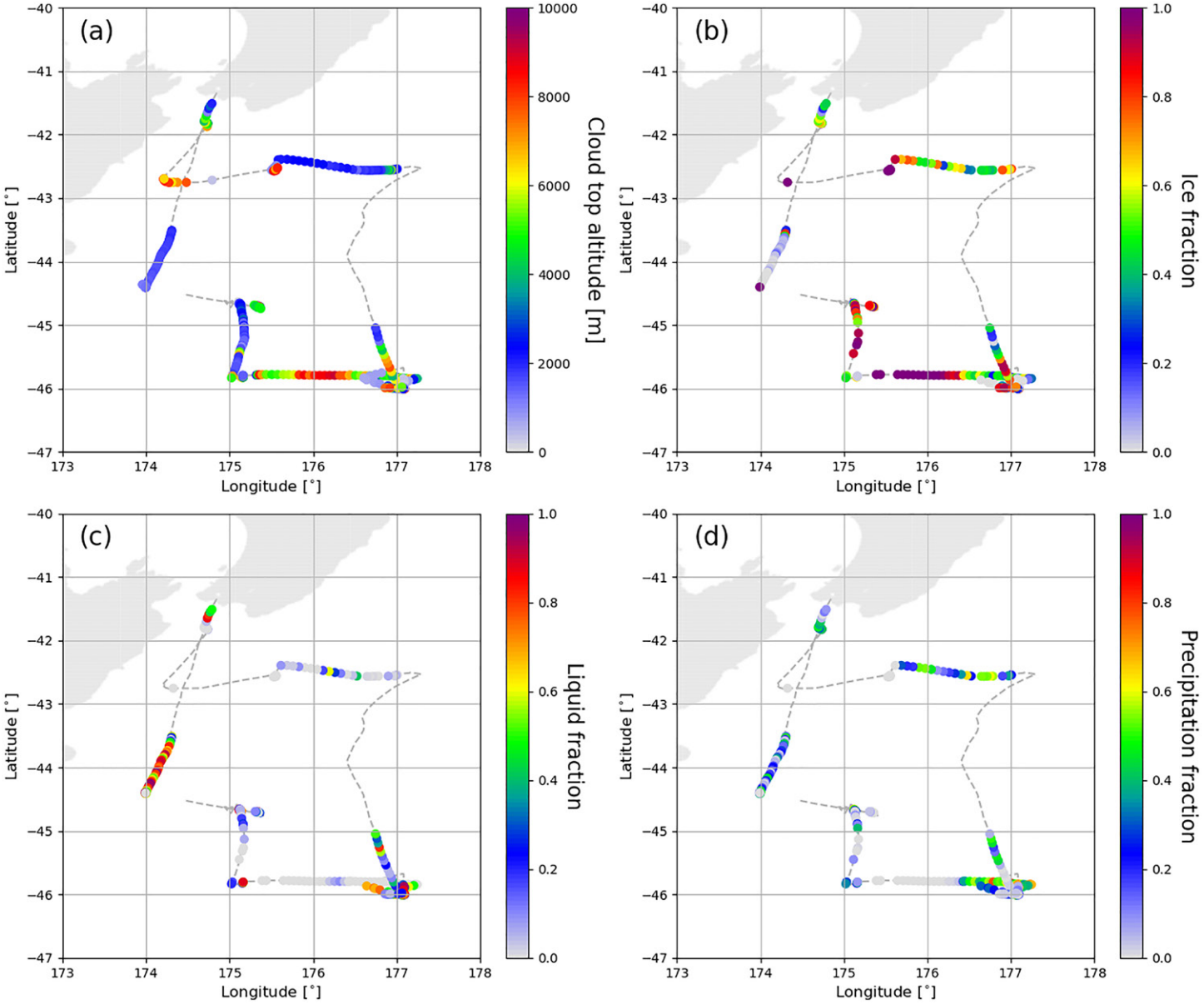

Fig. 16. The radar–lidar mask and target classification used to derive (a) cloud-top altitude, (b) ice fraction, (c) liquid fraction, and (d) precipitation fraction over the voyage track. The dashed line represents areas where radar was not scanning or lidar was not available.

Integration and extrapolation to the mesoscale

Combining new fluxes parameterizations, modeling, and ambient measurements. The general strategy of the Sea2Cloud project was to implement new marine aerosol source parameterizations developed from the ASIT and sea spray generation experiments and integrate these into mesoscale modeling exercises, then test their ability to reproduce aerosol and cloud spatial and temporal variability. For this, two modeling tools will be used, with WRF-Chem (Grell et al. 2005; Fast et al. 2006) applied to generate aerosol fields that will be adapted to initiate the DESCAM cloud-scale model (Flossmann and Wobrock 2010; Planche et al. 2010, 2014), which incorporates detailed microphysics (see also section S.3).

As a first step, the empirical relation reported by Sellegri et al. (2021) that relates the sea spray number flux to the nano- (2–20 μm) phytoplankton cell abundance, complemented by Sea2Cloud data, will be implemented in WRF-Chem, in addition to SSA number flux parameterizations already in the model (see section S.3.1). Nanophytoplankton cell abundance will be derived from satellite data (Uitz et al. 2006) as an input to the WRF-Chem Model. The ASIT experiments during Sea2Cloud provided further opportunity to investigate

the role of seawater biology in new particle formation, particularly, regarding the potential for an empirical formulation relating formation rate of newly formed particles to cell abundance of specific seawater phytoplanktonic groups, as with SSA.

In a second step, both the aerosol 3D mean field properties measured during the campaign or the ones obtained with WRF-Chem will be used in the DESCAM model to study the clouds' detailed microphysical properties. The DESCAM bin microphysics scheme is particularly suitable for studying aerosol–cloud interactions (Planche et al. 2010; Flossmann and Wobrock 2019; Kagkara et al. 2020; Arteaga et al. 2020). Five distributions are used to simulate the number of aerosol particles, cloud drops, and ice particles, plus aerosol mass inside cloud drops and ice particles. The aerosol particle activation into cloud droplets follows the Köhler theory and the heterogeneous ice nucleation is currently given by the approach of Meyers et al. (1992), which may be optimized using results from the Sea2Cloud campaign. The simulated aerosol and cloud fields will be evaluated using in situ and remote sensing ambient measurements. For comparison of WRF-Chem and DESCAM fields with the remote sensing observations, we will simulate the lidar and radar observations, using McRALI (Alkasem et al. 2017; Szczap et al. 2021), a Monte Carlo polarized lidar/radar Doppler simulator that accounts for multiple scattering processes, attenuation, Doppler effect, and the 3D structures of cloud and wind, for different instrumental configurations (sighting direction, field of view, ...). The advantage of such an approach is that model/observation discrepancies will be independent of assumptions in the remote sensing instrumentation inversions.

Regional analysis of satellite data. Spaceborne lidar and radar observations offer a unique opportunity to characterize the spatial and seasonal variability of clouds in remote environments such as the SO. Here, the synergy of *CALIPSO*/*CloudSat* measurements from 2007 to 2010 was exploited to assess the frequency of occurrence of the cloud phase based on the methodology described in Mioche et al. (2015). Version 2.2.3 of DARDAR MASK product was used to derive the cloud phase and type based on lidar and radar measurements merged on the same resolution grid (60 m vertical and 1.7 km horizontal) (Delanoë and Hogan 2008, 2010; Ceccaldi et al. 2013). The frequencies of occurrences were computed on a 2° latitude × 5° longitude grid between 40° and 60°S representing the SO, with the Sea2Cloud region (40°–50°S, 175°E–175°W). The analysis focused only on low-level clouds with altitude ranging between 500 m and 3 km in order to investigate the link between cloud properties and ocean biological activity. A way to investigate the percentage of clouds coupled to the surface is to calculate the difference of specific humidity (g kg^{-1}) between the lifting condensation level and the cloud base. Considering a threshold of 0.6 g kg^{-1} (Wang et al. 2016), we calculated that 50%–65% of the clouds are coupled with the ocean surface in the Sea2Cloud region.

Over the 4-yr period, DARDAR products indicated that the monthly averaged ice-containing cloud fraction (% relative to cold clouds) show a slight increase during late autumn (80%) over the SO. This seasonal variation is not observed when limiting the analysis to the South Pacific region where the Sea2Cloud voyage took place and where instead highest values are observed during summer (Fig. 17). We note that during summer, the highest ice-containing cloud fraction follows a geographical pattern similar to the one of the phytoplanktonic bloom along the Chatham Rise (Fig. 2). This could be due to ice nucleating properties of biological species present in this region. To further investigate the role of marine particle emissions on ice nucleation processes, we will use a statistical analysis at the regional scale of phase-classified low-level clouds in relation to satellite-derived products of the ocean biogeochemical properties such as particulate organic carbon (POC) (Sauzède et al. 2016), which was previously identified as the most effective tracer for marine INP concentrations in sea spray aerosol (Wilson et al. 2015; Trueblood et al. 2021). Extracting the biological marine aerosol influence from the meteorological influence will be achieved using a statistical

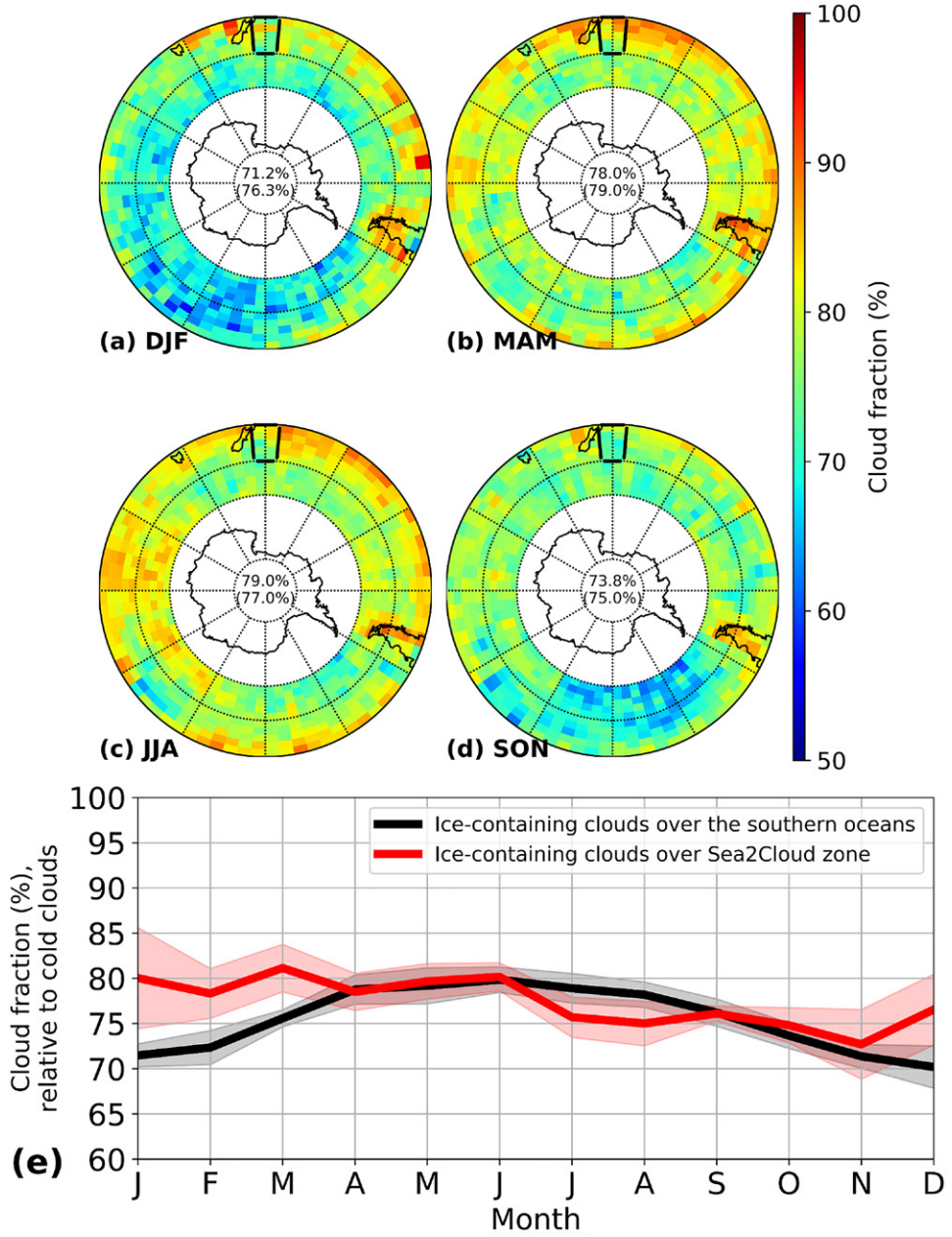

Fig. 17. Ice-containing cloud fraction (percent relative to cold clouds) over the SO from 2006 to 2017. (a)–(d) Seasonally segregated stereographic projections of the seasonal occurrence of ice containing clouds (with the Sea2Cloud campaign location represented in the black square). The averaged values for the whole SO and the Sea2Cloud region (in parentheses) are indicated in each panel. (e) Mean monthly fraction over the whole SO (black) and over the Sea2Cloud campaign region (red). The interannual variability (standard deviation) is represented by the shaded black and red areas.

approach at pseudo constant meteorological variables (Bazantay et al. 2023, manuscript submitted to *Geophys. Res. Lett.*).

Conclusions

The Sea2Cloud voyage was designed to answer process-orientated scientific questions related to air–sea interactions with a special focus on biologically initiated processes. To achieve this, a major effort focused on semicontrolled experiments aimed at simulating emission processes (secondary aerosol formation, sea spray generation) under near-natural environmental conditions representative of the surface SO. Special care was taken in preserving the natural biogeochemical complexity of surface seawater and maintaining ambient atmospheric environmental parameters such as temperature, light and oxidant levels, with a focus on

measuring selected variables with potential for parameterizing emission fluxes as a function of seawater biogeochemical properties in current models. The first results derived from the Sea2Cloud voyage show that biological processes influence physical and chemical emission fluxes to a large extent, and particularly aerosol properties related to cloud formation. We quantified biogenic emissions of trace gases under realistic environmental conditions and observed nucleation resulting from these biogenic seawater emissions in the ASITs. The recent finding by Peltola et al. (2022) at the New Zealand Baring Head GAW station showed that sub-10-nm particles in pristine marine air masses account for 30% of the total aerosol concentration. This implies that nucleation from similar biogenic vapors could contribute to increased CCN number concentrations upon growth of these particles. We also show sea spray generated via the plunging jet system continuously fed with the underway seawater produces sea spray fluxes containing 34% organic matter by mass, and that 4% of sea spray particles fluoresced with a strong signature characteristic of bacteria. We further confirmed that the cell abundance of nanophytoplankton in the seawater influenced sea spray number fluxes at sizes activated to cloud droplets at 0.2% sursaturation, as first evidenced by Sellegri et al. (2021). This is supporting an additional pathway for seawater biology to influence CCN sea–air fluxes. The aerosol size distribution in clean sectors of the Southern Ocean showed similar modes to that of nascent sea spray (nucleation, Aitken, two accumulation modes and two coarse modes), although with modes at larger sizes and a more pronounced Hoppel minimum, showing a strong impact of cloud processing. Our future strategy is to quantify the biological influence on emission fluxes for the different seawater types (subantarctic, subtropical, frontal), and the range of environmental conditions (representative of the austral autumn at these latitudes), and to evaluate its impact on cloud formation using the relationships derived from our experiments and a modeling approach. However, how marine microorganisms react to environmental variability is far from linear and unlikely to be universal across all seawater types and environmental conditions. Clearly, further studies are required, which incorporate process-based studies in other oceanic regions, with the goal of characterizing the conditions (oxidative stress, temperature change, grazing, viral lysis, etc.) that determine the influence of microorganisms on emissions of cloud forming particles to the atmosphere.

Acknowledgments. This research received funding from the European Research Council (ERC) under the Horizon 2020 research and innovation programme (Grant Agreement 771369), the Centre National des Etudes Spatiales (CNES), and was supported by NIWA SSIF funding to the Ocean-Climate Interactions, and Flows and Productivity Programmes. The Sea2Cloud project is endorsed by SOLAS. We acknowledge the support and expertise of the Officers and Crew of the R/V *Tangaroa* and NIWA Vessel Services. PJD and KAM acknowledge the U.S. National Science Foundation Grant AGS1660486, and KAM was additionally supported by an NSF Graduate Research Fellowship under Grant 006784. Any opinions, findings, and conclusions or recommendations expressed in this material are those of the author(s) and do not necessarily reflect the views of the National Science Foundation.

The ERA5 dataset is a Copernicus Products that has been generated under the framework of the Copernicus Climate Change Service (C3S). We acknowledge use of the WRF-Chem preprocessor tool (mozbc, fire_emiss, etc.) provided by the Atmospheric Chemistry Observations and Modeling Lab (ACOM) of NCAR. We acknowledge use of MOZART-4 global model output available at www.acom.ucar.edu/wrf-chem/mozart.shtml. We thank Tony Bromley and Sally Gray, NIWA, for assistance with the radiosonde system.

Data availability statement. All atmospheric and ocean datasets are accessible at https://sea2cloud.data-terra.org/en/catalogue/. The ERA5 meteorological data are provided by the following datasets: Hersbach et al. (2018a), DOI: 10.24381/cds.bd0915c6; and Hersbach et al. (2018b), DOI: 10.24381/cds.adbb2d47.

References

Alkasem, A., F. Szczap, C. Cornet, V. Shcherbakov, Y. Gour, and O. Jourdan, 2017: Effects of cirrus heterogeneity on lidar CALIOP/CALIPSO data. *J. Quant. Spectrosc. Radiat. Transfer*, **202**, 38–49, https://doi.org/10.1016/j.jqsrt.2017.07.005.

Andreae, M. O., W. Elbert, and S. J. de Mora, 1995: Biogenic sulfur emissions and aerosols over the tropical South Atlantic: 3. Atmospheric dimethylsulfide, aerosols and cloud condensation nuclei. *J. Geophys. Res.*, **100**, 11 335–11 356, https://doi.org/10.1029/94JD02828.

Arteaga, D., C. Planche, C. Kagkara, W. Wobrock, S. Banson, F. Tridon, and A. Flossmann, 2020: Evaluation of two cloud-resolving models using bin or bulk microphysics representation for the HyMeX-IOP7a heavy precipitation event. *Atmosphere*, **11**, 1177, https://doi.org/10.3390/atmos11111177.

Auger, M., R. Morrow, E. Kestenare, J.-B. Sallée, and R. Cowley, 2021: Southern Ocean in-situ temperature trends over 25 years emerge from interannual variability. *Nat. Commun.*, **12**, 514, https://doi.org/10.1038/s41467-020-20781-1.

Ayers, G., and J. Gras, 1991: Seasonal relationship between cloud condensation nuclei and aerosol methanesulphonate in marine air. *Nature*, **353**, 834–835, https://doi.org/10.1038/353834a0.

Baccarini, A., J. Dommen, K. Lehtipalo, S. Henning, R. L. Modini, M. Gysel-Beer, U. Baltensperger, and J. Schmale, 2021: Low-volatility vapors and new particle formation over the Southern Ocean during the Antarctic Circumnavigation Expedition. *J. Geophys. Res. Atmos.*, **126**, e2021JD035126, https://doi.org/10.1029/2021JD035126.

Bian, H., and Coauthors, 2019: Observationally constrained analysis of sea salt aerosol in the marine atmosphere. *Atmos. Chem. Phys.*, **19**, 10 773–10 785, https://doi.org/10.5194/acp-19-10773-2019.

Bigg, E. K., and C. Leck, 2008: The composition of fragments of bubbles bursting at the ocean surface. *J. Geophys. Res.*, **113**, D11209, https://doi.org/10.1029/2007JD009078.

——, J. Gras, and C. Evans, 1984: Origin of Aitken particles in remote regions of the Southern Hemisphere. *J. Atmos. Chem.*, **1**, 203–214, https://doi.org/10.1007/BF00053841.

Blake, R. S., P. S. Monks, and A. M. Ellis, 2009: Proton-transfer reaction mass spectrometry. *Chem. Rev.*, **109**, 861–896, https://doi.org/10.1021/cr800364q.

Bodas-Salcedo, A., K. D. Williams, P. R. Field, and A. P. Lock, 2012: The surface downwelling solar radiation surplus over the Southern Ocean in the Met Office model: The role of midlatitude cyclone clouds. *J. Climate*, **25**, 7467–7486, https://doi.org/10.1175/JCLI-D-11-00702.1.

——, J. P. Mulcahy, T. Andrews, K. D. Williams, M. A. Ringer, P. R. Field, and G. S. Elsaesser, 2019: Strong dependence of atmospheric feedbacks on mixed-phase microphysics and aerosol-cloud interactions in HadGEM3. *J. Adv. Model. Earth Syst.*, **11**, 1735–1758, https://doi.org/10.1029/2019MS001688.

Bopp, L., O. Aumont, S. Belviso, and P. Monfray, 2003: Potential impact of climate change on marine dimethyl sulfide emissions. *Tellus*, **55B**, 11–22, https://doi.org/10.3402/tellusb.v55i1.16359.

Boucher, O., and Coauthors, 2003: DMS atmospheric concentrations and sulphate aerosol indirect radiative forcing: A sensitivity study to the DMS source representation and oxidation. *Atmos. Chem. Phys.*, **3**, 49–65, https://doi.org/10.5194/acp-3-49-2003.

Burrows, S. M., C. Hoose, U. Pöschl, and M. G. Lawrence, 2013: Ice nuclei in marine air: Biogenic particles or dust? *Atmos. Chem. Phys.*, **13**, 245–267, https://doi.org/10.5194/acp-13-245-2013.

——, R. Easter, X. Liu, P.-L. Ma, H. Wang, S. M. Elliott, B. Singh, K. Zhang, and P. J. Rasch, 2022: OCEANFILMS (Organic Compounds from Ecosystems to Aerosols: Natural Films and Interfaces via Langmuir Molecular Surfactants) sea spray organic aerosol emissions—Implementation in a global climate model and impacts on clouds. *Atmos. Chem. Phys.*, **22**, 5223–5251, https://doi.org/10.5194/acp-22-5223-2022.

Carpenter, L. J., S. M. MacDonald, M. D. Shaw, R. Kumar, R. W. Saunders, R. Parthipan, J. Wilson, and J. M. C. Plane, 2013: Atmospheric iodine levels influenced by sea surface emissions of inorganic iodine. *Nat. Geosci.*, **6**, 108–111, https://doi.org/10.1038/ngeo1687.

Ceccaldi, M., J. Delanoë, R. J. Hogan, N. L. Pounder, A. Protat, and J. Pelon, 2013: From CloudSat-CALIPSO to EarthCARE: Evolution of the DARDAR cloud classification and its comparison to airborne radar-lidar observations. *J. Geophys. Res. Atmos.*, **118**, 7962–7981, https://doi.org/10.1002/jgrd.50579.

Chang, F. H., and M. Gall, 1998: Phytoplankton assemblages and photosynthetic pigments during winter and spring in the subtropical convergence region near New Zealand. *N. Z. J. Mar. Freshwater Res.*, **32**, 515–530, https://doi.org/10.1080/00288330.1998.9516840.

Charlson, R. J., J. E. Lovelock, M. O. Andreae, and S. G. Warren, 1987: Oceanic phytoplankton, atmospheric sulphur, cloud albedo and climate. *Nature*, **326**, 655–661, https://doi.org/10.1038/326655a0.

Chiswell, S. M., H. C. Bostock, P. J. H. Sutton, and M. J. M. Williams, 2015: Physical oceanography of the deep seas around New Zealand: A review. *N. Z. J. Mar. Freshwater Res.*, **49**, 286–317, https://doi.org/10.1080/00288330.2014.992918.

Clarke, A. D., and V. N. Kapustin, 2002: A Pacific aerosol survey. Part I: A decade of data on particle production, transport, evolution, and mixing in the troposphere. *J. Atmos. Sci.*, **59**, 363–382, https://doi.org/10.1175/1520-0469(2002)059<0363:APASPI>2.0.CO;2.

——, and Coauthors, 1998: Particle nucleation in the tropical boundary layer and its coupling to marine sulfur sources. *Science*, **282**, 89–92, https://doi.org/10.1126/science.282.5386.89.

Cooper, O. R., and Coauthors, 2020: Multi-decadal surface ozone trends at globally distributed remote locations. *Elementa*, **8**, 23, https://doi.org/10.1525/elementa.420.

Covert, D. S., V. N. Kapustin, P. K. Quinn, and T. S. Bates, 1992: New particle formation in the marine boundary layer. *J. Geophys. Res.*, **97**, 20 581–20 589, https://doi.org/10.1029/92JD02074.

Cravigan, L., and Coauthors, 2020: Sea spray aerosol organic enrichment, water uptake and surface tension effects. *Atmos. Chem. Phys.*, **20**, 7955–7977, https://doi.org/10.5194/acp-20-7955-2020.

Cuevas, C. A., and Coauthors, 2018: Rapid increase in atmospheric iodine levels in the North Atlantic since the mid-20th century. *Nat. Commun.*, **9**, 1452, https://doi.org/10.1038/s41467-018-03756-1.

Cunliffe, M., and J. C. Murrell, 2009: The sea-surface microlayer is a gelatinous biofilm. *ISME J.*, **3**, 1001–1003, https://doi.org/10.1038/ismej.2009.69.

——, and Coauthors, 2013: Sea surface microlayers: A unified physicochemical and biological perspective of the air–ocean interface. *Prog. Oceanogr.*, **109**, 104–116, https://doi.org/10.1016/j.pocean.2012.08.004.

Delanoë, J., and R. J. Hogan, 2008: A variational scheme for retrieving ice cloud properties from combined radar, lidar, and infrared radiometer. *J. Geophys. Res.*, **113**, D07204, https://doi.org/10.1029/2007JD009000.

——, and ——, 2010: Combined CloudSat-CALIPSO-MODIS retrievals of the properties of ice clouds. *J. Geophys. Res.*, **115**, D00H29, https://doi.org/10.1029/2009JD012346.

Delizo, L., W. O. Smith, and J. Hall, 2007: Taxonomic composition and growth rates of phytoplankton assemblages at the subtropical convergence east of New Zealand. *J. Plankton Res.*, **29**, 655–670, https://doi.org/10.1093/plankt/fbm047.

DeMott, P. J., and Coauthors, 2016: Sea spray aerosol as a unique source of ice nucleating particles. *Proc. Natl. Acad. Sci. USA*, **113**, 5797–5803, https://doi.org/10.1073/pnas.1514034112.

Edtbauer, A., C. Stönner, E. Y. Pfannerstill, M. Berasategui, D. Walter, J. N. Crowley, J. Lelieveld, and J. Williams, 2020: A new marine biogenic emission: Methane sulfonamide (MSAM), dimethyl sulfide (DMS), and dimethyl sulfone ($DMSO_2$) measured in air over the Arabian Sea. *Atmos. Chem. Phys.*, **20**, 6081–6094, https://doi.org/10.5194/acp-20-6081-2020.

Engel, A., and Coauthors, 2017: The ocean's vital skin: Toward an integrated understanding of the sea surface microlayer. *Front. Mar. Sci.*, **4**, 165, https://doi.org/10.3389/fmars.2017.00165.

——, M. Sperling, C. Sun, J. Grosse, and G. Friedrichs, 2018: Organic matter in the surface microlayer: Insights from a wind wave channel experiment. *Front. Mar. Sci.*, **5**, 182, https://doi.org/10.3389/fmars.2018.00182.

Fast, J. D., W. I. Gustafson Jr., R. C. Easter Jr., R. A. Zaveri, J. C. Barnard, E. G. Chapman, G. Grell, and S. E. Peckham, 2006: Evolution of ozone, particulates, and aerosol direct radiative forcing in the vicinity of Houston using a fully coupled meteorology–chemistry–aerosol model. *J. Geophys. Res.*, **111**, D21305, https://doi.org/10.1029/2005JD006721.

Fitzgerald, J. W., 1991: Marine aerosols: A review. *Atmos. Environ.*, **25**, 533–545, https://doi.org/10.1016/0960-1686(91)90050-H.

Flossmann, A. I., and W. Wobrock, 2010: A review of our understanding of the aerosol–cloud interaction from the perspective of a bin resolved cloud scale modelling. *Atmos. Res.*, **97**, 478–497, https://doi.org/10.1016/j.atmosres.2010.05.008.

——, and ——, 2019: Cloud processing of aerosol particles in marine stratocumulus clouds. *Atmosphere*, **10**, 520, https://doi.org/10.3390/atmos10090520.

Forestieri, S. D., K. A. Moore, R. Martinez Borrero, A. Wang, M. D. Stokes, and C. D. Cappa, 2018: Temperature and composition dependence of sea spray aerosol production. *Geophys. Res. Lett.*, **45**, 7218–7225, https://doi.org/10.1029/2018GL078193.

Freney, E., and Coauthors, 2021: Mediterranean nascent sea spray organic aerosol and relationships with seawater biogeochemistry. *Atmos. Chem. Phys.*, **21**, 10 625–10 641, https://doi.org/10.5194/acp-21-10625-2021.

Fuentes, E., H. Coe, D. Green, G. de Leeuw, and G. McFiggans, 2010: On the impacts of phytoplankton-derived organic matter on the properties of the primary marine aerosol—Part 1: Source fluxes. *Atmos. Chem. Phys.*, **10**, 9295–9317, https://doi.org/10.5194/acp-10-9295-2010.

Gabric, A. J., R. Cropp, G. P. Ayers, G. McTainsh, and R. Braddock, 2002: Coupling between cycles of phytoplankton biomass and aerosol optical depth as derived from SeaWiFS time series in the sub-Antarctic Southern Ocean. *Geophys. Res. Lett.*, **29**, 1112, https://doi.org/10.1029/2001GL013545.

Galgani, L., and A. Engel, 2016: Changes in optical characteristics of surface microlayers hint to photochemically and microbially mediated DOM turnover in the upwelling region off the coast of Peru. *Biogeosciences*, **13**, 2453–2473, https://doi.org/10.5194/bg-13-2453-2016.

Gantt, B., and N. Meskhidze, 2013: The physical and chemical characteristics of marine primary organic aerosol: A review. *Atmos. Chem. Phys.*, **13**, 3979–3996, https://doi.org/10.5194/acp-13-3979-2013.

Grell, G. A., S. E. Peckham, R. Schmitz, S. A. McKeen, G. Frost, W. C. Skamarock, and B. Eder, 2005: Fully coupled online chemistry within the WRF Model. *Atmos. Environ.*, **39**, 6957–6975, https://doi.org/10.1016/j.atmosenv.2005.04.027.

Hara, K., C. Nishita-Hara, K. Osada, M. Yabuki, and T. Yamanouchi, 2021: Characterization of aerosol number size distributions and their effect on cloud properties at Syowa Station, Antarctica. *Atmos. Chem. Phys.*, **21**, 12 155–12 172, https://doi.org/10.5194/acp-21-12155-2021.

Hegg, D. A., R. J. Ferek, P. V. Hobbs, and L. F. Radke, 1991: Dimethyl sulfide and cloud condensation nucleus correlations in the northeast Pacific Ocean. *J. Geophys. Res.*, **96**, 13 189–13 191, https://doi.org/10.1029/91JD01309.

Hersbach, H., and Coauthors, 2018a: ERA5 hourly data on pressure levels from 1979 to present. C3S CDS, accessed 8 June 2020, https://doi.org/10.24381/cds.bd0915c6.

——, and Coauthors, 2018b: ERA5 hourly data on single levels from 1979 to present. C3S CDS, accessed 8 June 2020, https://doi.org/10.24381/cds.adbb2d47.

Hodshire, A. L., P. Campuzano-Jost, J. K. Kodros, B. Croft, B. A. Nault, J. C. Schroder, J. L. Jimenez, and J. R. Pierce, 2019: The potential role of methanesulfonic acid (MSA) in aerosol formation and growth and the associated radiative forcings. *Atmos. Chem. Phys.*, **19**, 3137–3160, https://doi.org/10.5194/acp-19-3137-2019.

Humphries, R. S., and Coauthors, 2021: Southern Ocean latitudinal gradients of cloud condensation nuclei. *Atmos. Chem. Phys.*, **21**, 12 757–12 782, https://doi.org/10.5194/acp-21-12757-2021.

Hunter, K. A., 1980: Processes affecting particulate trace metals in the sea surface microlayer. *Mar. Chem.*, **9**, 49–70, https://doi.org/10.1016/0304-4203(80)90006-7.

Inamdar, S., and Coauthors, 2020: Estimation of reactive inorganic iodine fluxes in the Indian and Southern Ocean marine boundary layer. *Atmos. Chem. Phys.*, **20**, 12 093–12 114, https://doi.org/10.5194/acp-20-12093-2020.

Jokinen, and Coauthors, 2012: Atmospheric sulfuric acid and neutral cluster measurements using CI-APi-TOF. *Atmos. Chem. Phys.*, **12**, 4117–4125, https://doi.org/10.5194/acp-12-4117-2012.

Junninen, H., and Coauthors, 2010: A high-resolution mass spectrometer to measure atmospheric ion composition. *Atmos. Meas. Tech.*, **3**, 1039–1053, https://doi.org/10.5194/amt-3-1039-2010.

Kagkara, C., W. Wobrock, C. Planche, and A. Flossmann, 2020: The sensitivity of intense rainfall to aerosol particle loading—A comparison of bin-resolved microphysics modeling with observations of heavy precipitation from HyMeX IOP7a. *Nat. Hazards Earth Syst. Sci.*, **20**, 1469–1483, https://doi.org/10.5194/nhess-20-1469-2020.

Kawana, K., K. Matsumoto, F. Taketani, T. Miyakawa, and Y. Kanaya, 2021: Fluorescent biological aerosol particles over the central Pacific Ocean: Covariation with ocean surface biological activity indicators. *Atmos. Chem. Phys.*, **21**, 15 969–15 983, https://doi.org/10.5194/acp-21-15969-2021.

Kirkby, J., and Coauthors, 2011: Role of sulphuric acid, ammonia and galactic cosmic rays in atmospheric aerosol nucleation. *Nature*, **476**, 429–433, https://doi.org/10.1038/nature10343.

Korhonen, H., K. S. Carslaw, D. V. Spracklen, G. W. Mann, and M. T. Woodhouse, 2008: Influence of oceanic dimethyl sulfide emissions on cloud condensation nuclei concentrations and seasonality over the remote Southern Hemisphere oceans: A global model study. *J. Geophys. Res.*, **113**, D15204, https://doi.org/10.1029/2007JD009718.

Kürten, A., and Coauthors, 2014: Neutral molecular cluster formation of sulfuric acid–dimethylamine observed in real time under atmospheric conditions. *Proc. Natl. Acad. Sci. USA*, **111**, 15 019–15 024, https://doi.org/10.1073/pnas.1404853111.

Kuznetsova, M., and C. Lee, 2001: Enhanced extracellular enzymatic peptide hydrolysis in the sea-surface microlayer. *Mar. Chem.*, **73**, 319–332, https://doi.org/10.1016/S0304-4203(00)00116-X.

Langematz, U., 2018: Future ozone in a changing climate. *C. R. Geosci.*, **350**, 403–409, https://doi.org/10.1016/j.crte.2018.06.015.

Langmann, B., C. Scannell, and C. O'Dowd, 2008: New directions: Organic matter contribution to marine aerosols and cloud condensation nuclei. *Atmos. Environ.*, **42**, 7821–7822, https://doi.org/10.1016/j.atmosenv.2008.09.002.

Law, C. S., and Coauthors, 2017: Overview and preliminary results of the Surface Ocean Aerosol Production (SOAP) campaign. *Atmos. Chem. Phys.*, **17**, 13 645–13 667, https://doi.org/10.5194/acp-17-13645-2017.

Legrand, M., and Coauthors, 2018: Alpine ice evidence of a three-fold increase in atmospheric iodine deposition since 1950 in Europe due to increasing oceanic emissions. *Proc. Natl. Acad. Sci. USA*, **115**, 12 136–12 141, https://doi.org/10.1073/pnas.1809867115.

Lindinger, W., A. Hansel, and A. Jordan, 1998: On-line monitoring of volatile organic compounds at PPTV levels by means of proton-transfer-reaction mass spectrometry (PTR-MS) medical applications, food control and environmental research. *Int. J. Mass Spectrom. Ion Processes*, **173**, 191–241, https://doi.org/10.1016/S0168-1176(97)00281-4.

Lion, L. W., and J. O. Leckie, 1981: The biogeochemistry of the air-sea interface. *Annu. Rev. Earth Planet. Sci.*, **9**, 449–486, https://doi.org/10.1146/annurev.ea.09.050181.002313.

MacDonald, S. M., J. C. Gómez Martín, R. Chance, S. Warriner, A. Saiz-Lopez, L. J. Carpenter, and J. M. C. Plane, 2014: A laboratory characterisation of inorganic iodine emissions from the sea surface: Dependence on oceanic variables and parameterisation for global modelling. *Atmos. Chem. Phys.*, **14**, 5841–5852, https://doi.org/10.5194/acp-14-5841-2014.

Mari, X., U. Passow, C. Migon, A. B. Burd, and L. Legendre, 2017: Transparent exopolymer particles: Effects on carbon cycling in the ocean. *Prog. Oceanogr.*, **151**, 13–37, https://doi.org/10.1016/j.pocean.2016.11.002.

McCluskey, C. S., and Coauthors, 2018a: Marine and terrestrial organic ice-nucleating particles in pristine marine to continentally influenced northeast Atlantic air masses. *J. Geophys. Res. Atmos.*, **123**, 6196–6212, https://doi.org/10.1029/2017JD028033.

——, and Coauthors, 2018b: A mesocosm double feature: Insights into the chemical makeup of marine ice nucleating particles. *J. Atmos. Sci.*, **75**, 2405–2423, https://doi.org/10.1175/JAS-D-17-0155.1.

McCoy, I. L., and Coauthors, 2020: The hemispheric contrast in cloud microphysical properties constrains aerosol forcing. *Proc. Natl. Acad. Sci. USA*, **117**, 18 998–19 006, https://doi.org/10.1073/pnas.1922502117.

McFarquhar, G. M., and Coauthors, 2021, Observations of clouds, aerosols, precipitation, and surface radiation over the Southern Ocean: An overview of CAPRICORN, MARCUS, MICRE, and SOCRATES. *Bull. Amer. Meteor. Soc.*, **102**, E894–E928, https://doi.org/10.1175/BAMS-D-20-0132.1.

McFiggans, G., and Coauthors, 2004: Direct evidence for coastal iodine particles from Laminaria macroalgae—Linkage to emissions of molecular iodine. *Atmos. Chem. Phys.*, **4**, 701–713, https://doi.org/10.5194/acp-4-701-2004.

Merikanto, J., D. V. Spracklen, G. W. Mann, S. J. Pickering, and K. S. Carslaw, 2009: Impact of nucleation on global CCN. *Atmos. Chem. Phys.*, **9**, 8601–8616, https://doi.org/10.5194/acp-9-8601-2009.

Meyers, M. P., P. J. Demott, and W. R. Cotton, 1992: New primary ice nucleation parameterizations in an explicit cloud model. *J. Appl. Meteor.*, **31**, 708–721, https://doi.org/10.1175/1520-0450(1992)031<0708:NPINPI>2.0.CO;2.

Mioche, G., O. Jourdan, M. Ceccaldi, and J. Delanoë, 2015: Variability of mixed-phase clouds in the Arctic with a focus on the Svalbard region: A study based on spaceborne active remote sensing. *Atmos. Chem. Phys.*, **15**, 2445–2461, https://doi.org/10.5194/acp-15-2445-2015.

Miranda, M. L., N. I. H. Mustaffa, T. B. Robinson, C. Stolle, M. Ribas-Ribas, O. Wurl, and O. Zielinski, 2018: Influence of solar radiation on biogeochemical parameters and fluorescent dissolved organic matter (FDOM) in the sea surface microlayer of the southern coastal North Sea. *Elementa*, **6**, 15, https://doi.org/10.1525/elementa.278.

Moallemi, A., and Coauthors, 2021: Sources, occurrence and characteristics of fluorescent biological aerosol particles measured over the pristine Southern Ocean. *J. Geophys. Res. Atmos.*, **126**, e2021JD034811, https://doi.org/10.1029/2021JD034811.

Murphy, R. J., M. H. Pinkerton, K. M. Richardson, J. M. Bradford-Grieve, and P. W. Boyd, 2001: Phytoplankton distributions around New Zealand derived from SeaWiFS remotely-sensed ocean colour data. *N. Z. J. Mar. Freshwater Res.*, **35**, 343–362, https://doi.org/10.1080/00288330.2001.9517005.

O'Dowd, C. D., J. A. Lowe, M. H. Smith, B. Davidson, C. N. Hewitt, and R. M. Harrison, 1997: Biogenic sulphur emissions and inferred non-sea-salt-sulphate cloud condensation nuclei in and around Antarctica. *J. Geophys. Res.*, **102**, 12 839–12 854, https://doi.org/10.1029/96JD02749.

——, and Coauthors, 2002a: Coastal new particle formation: Environmental conditions and aerosol physicochemical characteristics during nucleation bursts. *J. Geophys. Res.*, **107**, 8107, https://doi.org/10.1029/2000JD000206.

——, and Coauthors, 2002b: Marine aerosol formation from biogenic iodine emissions. *Nature*, **417**, 632–636, https://doi.org/10.1038/nature00775.

——, B. Langmann, S. Varghese, C. Scannell, D. Ceburnis, and M. C. Facchini, 2008: A combined organic-inorganic sea-spray source function. *Geophys. Res. Lett.*, **35**, L01801, https://doi.org/10.1029/2007GL030331.

——, C. Monahan, and M. Dall'Osto, 2010: On the occurrence of open ocean particle production and growth events. *Geophys. Res. Lett.*, **37**, L19805, https://doi.org/10.1029/2010GL044679.

Ovadnevaite, J., and Coauthors, 2017: Surface tension prevails over solute effect in organic-influenced cloud droplet activation. *Nature*, **546**, 637–641, https://doi.org/10.1038/nature22806.

Peltola, M., C. Rose, J. V. Trueblood, S. Gray, M. Harvey, and K. Sellegri, 2022: New particle formation in coastal New Zealand with a focus on open-ocean air masses. *Atmos. Chem. Phys.*, **22**, 6231–6254, https://doi.org/10.5194/acp-22-6231-2022.

Perring, A. E., J. P. Schwarz, D. Baumgardner, M. T. Hernandez, D. V. Spracklen, and C. L. Heald, 2015: Airborne observations of regional variation in fluorescent aerosol across the United States. *J. Geophys. Res. Atmos.*, **120**, 1153–1170, https://doi.org/10.1002/2014JD022495.

Planche, C., W. Wobrock, A. I. Flossmann, F. Tridon, J. Van Baelen, Y. Pointin, and M. Hagen, 2010: The influence of aerosol particle number and hygroscopicity on the evolution of convective cloud systems and their precipitation: A numerical study based on the COPS observations on 12 August 2007. *Atmos. Res.*, **98**, 40–56, https://doi.org/10.1016/j.atmosres.2010.05.003.

——, ——, and ——, 2014: The continuous melting process in a cloud scale model using a bin microphysics scheme. *Quart. J. Roy. Meteor. Soc.*, **140**, 1986–1996, https://doi.org/10.1002/qj.2265.

Prados-Roman, C., C. A. Cuevas, R. P. Fernandez, D. E. Kinnison, J.-F. Lamarque, and A. Saiz-Lopez, 2015: A negative feedback between anthropogenic ozone pollution and enhanced ocean emissions of iodine. *Atmos. Chem. Phys.*, **15**, 2215–2224, https://doi.org/10.5194/acp-15-2215-2015.

Protat, A., E. Schulz, L. Rikus, Z. Sun, Y. Xiao, and M. Keywood, 2017: Shipborne observations of the radiative effect of Southern Ocean clouds. *J. Geophys. Res. Atmos.*, **122**, D026061, https://doi.org/10.1002/2016JD026061.

Quinn, P., and T. S. Bates, 2011: The case against climate regulation via oceanic phytoplankton sulphur emissions. *Nature*, **480**, 51–56, https://doi.org/10.1038/nature10580.

Regayre, L. A., and Coauthors, 2020: The value of remote marine aerosol measurements for constraining radiative forcing uncertainty. *Atmos. Chem. Phys.*, **20**, 10 063–10 072, https://doi.org/10.5194/acp-20-10063-2020.

Rocco, M., and Coauthors, 2021: Oceanic phytoplankton are a potentially important source of benzenoids to the remote marine atmosphere. *Nat. Commun. Earth Environ.*, **2**, 175, https://doi.org/10.1038/s43247-021-00253-0.

——, and Coauthors, 2023: Air-sea fluxes of dimethyl sulphide and methanethiol in the south-west Pacific. *EGUsphere*, https://doi.org/10.5194/egusphere-2023-516.

Rolph, G., A. Stein, and B. Stunder, 2017: Real-time Environmental Applications and Display System: READY. *Environ. Modell. Software*, **95**, 210–228, https://doi.org/10.1016/j.envsoft.2017.06.025.

Rose, C., and Coauthors, 2015: Airborne measurements of new particle formation in the free troposphere above the Mediterranean Sea during the HYMEX campaign. *Atmos. Chem. Phys.*, **15**, 10 203–10 218, https://doi.org/10.5194/acp-15-10203-2015.

Saiz-Lopez, A., and J. M. C. Plane, 2004: Novel iodine chemistry in the marine boundary layer. *Geophys. Res. Lett.*, **31**, L04112, https://doi.org/10.1029/2003GL019215.

——, ——, A. R. Baker, L. J. Carpenter, R. von Glasow, J. C. Gómez Martín, G. McFiggans, and R. W. Saunders, 2012: Atmospheric chemistry of iodine. *Chem. Rev.*, **112**, 1773–1804, https://doi.org/10.1021/cr200029u.

Salter, M. E., P. Zieger, J. C. Acosta Navarro, H. Grythe, A. Kirkevåg, B. Rosati, I. Riipinen, and E. D. Nilsson, 2015: An empirically derived inorganic sea spray source function incorporating sea surface temperature. *Atmos. Chem. Phys.*, **15**, 11 047–11 066, https://doi.org/10.5194/acp-15-11047-2015.

Santos, A. L., V. Oliveira, I. Baptista, I. Henriques, N. C. M. Gomes, A. Almeida, A. Correia, and A. Cunha, 2012: Effects of UV-B radiation on the structural and physiological diversity of bacterioneuston and bacterioplankton. *Appl. Environ. Microbiol.*, **78**, 2066–2069, https://doi.org/10.1128/AEM.06344-11.

Sauzède, R., and Coauthors, 2016: A neural network-based method for merging ocean color and Argo data to extend surface bio-optical properties to depth: Retrieval of the particulate backscattering coefficient. *J. Geophys. Res. Oceans*, **121**, 2552–2571, https://doi.org/10.1002/2015JC011408.

Savage, N. J., C. E. Krentz, T. Könemann, T. T. Han, G. Mainelis, C. Pöhlker, and J. A. Huffman, 2017: Systematic characterization and fluorescence threshold strategies for the Wideband Integrated Bioaerosol Sensor (WIBS) using size-resolved biological and interfering particles. *Atmos. Meas. Tech.*, **10**, 4279–4302, https://doi.org/10.5194/amt-10-4279-2017.

Schlitzer, R., 2020: Ocean Data View. AWI, accessed DD MMM YYYY, https://odv.awi.de/.

Schmale, J., and Coauthors, 2019: Overview of the Antarctic Circumnavigation Expedition: Study of Preindustrial-like Aerosols and their Climate Effects (ACE-SPACE). *Bull. Amer. Meteor. Soc.*, **11**, 2260–2283, https://doi.org/10.1175/BAMS-D-18-0187.1.

Schwier, A. N., and Coauthors, 2015: Primary marine aerosol emissions from the Mediterranean Sea during pre-bloom and oligotrophic conditions: Correlations to seawater chlorophyll *a* from a mesocosm study. *Atmos. Chem. Phys.*, **15**, 7961–7976, https://doi.org/10.5194/acp-15-7961-2015.

——, and Coauthors, 2017: Primary marine aerosol physical and chemical emissions during a nutriment enrichment experiment in mesocosms of the Mediterranean Sea. *Atmos. Chem. Phys.*, **17**, 14645–14660, https://doi.org/10.5194/acp-17-14645-2017.

Sciare, J., O. Favez, R. Sarda-Estève, K. Oikonomou, H. Cachier, and V. Kazan, 2009: Long-term observations of carbonaceous aerosols in the austral ocean atmosphere: Evidence of a biogenic marine organic source. *J. Geophys. Res.*, **114**, D15302, https://doi.org/10.1029/2009JD011998.

Seinfeld, J. H., and S. N. Pandis, 2006: *Atmospheric Chemistry and Physics: From Air Pollution to Climate Change.* John Wiley and Sons, 1152 pp.

Sellegri, K., Y. J. Yoon, S. G. Jennings, C. D. O'Dowd, L. Pirjola, S. Cautenet, and H. Chen, 2005: Quantification of coastal new ultra-fine particles formation from in situ and chamber measurements during the BIOFLUX campaign. *Environ. Chem.*, **2**, 260, https://doi.org/10.1071/EN05074.

——, C. D. O'Dowd, Y. J. Yoon, S. G. Jennings, and G. de Leeuw, 2006: Surfactants and submicron sea spray generation. *J. Geophys. Res.*, **111**, D22215, https://doi.org/10.1029/2005JD006658.

——, and Coauthors, 2016: Evidence of atmospheric nanoparticle formation from emissions of marine microorganisms. *Geophys. Res. Lett.*, **43**, 6596–6603, https://doi.org/10.1002/2016GL069389.

——, and Coauthors, 2021: Surface ocean microbiota determine cloud precursors. *Sci. Rep.*, **11**, 281, https://doi.org/10.1038/s41598-020-78097-5.

——, and Coauthors, 2022: Quantified effect of seawater biogeochemistry on the temperature dependence of sea spray aerosol fluxes. *Atmos. Chem. Phys. Discuss.*, https://doi.org/10.5194/acp-2022-790.

Sieburth, J. M., 1983: Microbiological and organic-chemical processes in the surface and mixed layers. *Air-Sea Exchange of Gases and Particles*, P. S. Liss and W. G. N. Slinn, Eds., Springer, 121–172, https://doi.org/10.1007/978-94-009-7169-1_3.

Sipilä, M., and Coauthors, 2016: Molecular-scale evidence of aerosol particle formation via sequential addition of HIO_3. *Nature*, **537**, 532–534, https://doi.org/10.1038/nature19314.

Smith, M. J., D. T. Ho, C. S. Law, J. McGregor, S. Popinet, and P. Schlosser, 2011: Uncertainties in gas exchange parameterisation during the SAGE dual-tracer experiment. *Deep-Sea Res. II*, **58**, 869–881, https://doi.org/10.1016/j.dsr2.2010.10.025.

Sorooshian, A., and Coauthors, 2009: On the link between ocean biota emissions, aerosol, and maritime clouds: Airborne, ground, and satellite measurements off the coast of California. *Global Biogeochem. Cycles*, **23**, GB4007, https://doi.org/10.1029/2009GB003464.

Szczap, F., and Coauthors, 2021: McRALI: A Monte Carlo high-spectral-resolution lidar and Doppler radar simulator for three-dimensional cloudy atmosphere remote sensing. *Atmos. Meas. Tech.*, **14**, 199–221, https://doi.org/10.5194/amt-14-199-2021.

Tatzelt, C., and Coauthors, 2022: Circum-Antarctic abundance and properties of CCN and INP. *Atmos. Chem. Phys.*, **22**, 9721–9745, https://doi.org/10.5194/acp-22-9721-2022.

Thorenz, U. R., L. J. Carpenter, R.-J. Huang, M. Kundel, J. Bosle, and T. Hoffmann, 2014: Emission of iodine-containing volatiles by selected microalgae species. *Atmos. Chem. Phys.*, **14**, 13327–13335, https://doi.org/10.5194/acp-14-13327-2014.

Trueblood, J. V., and Coauthors, 2021: A two-component parameterization of marine ice-nucleating particles based on seawater biology and sea spray aerosol measurements in the Mediterranean Sea. *Atmos. Chem. Phys.*, **21**, 4659–4676, https://doi.org/10.5194/acp-21-4659-2021.

Uitz, J., H. Claustre, A. Morel, and S. B. Hooker, 2006: Vertical distribution of phytoplankton communities in open ocean: An assessment based on surface chlorophyll. *J. Geophys. Res.*, **111**, C08005, https://doi.org/10.1029/2005JC003207.

Vallina, S. M., R. Simó, and S. Gasso, 2006: What controls CCN seasonality in the Southern Ocean? A statistical analysis based on satellite-derived chlorophyll and CCN and model-estimated OH radical and rainfall. *Global Biogeochem. Cycles*, **20**, GB1014, https://doi.org/10.1029/2005GB002597.

van Pinxteren, M., and Coauthors, 2020: Marine organic matter in the remote environment of the Cape Verde islands—An introduction and overview to the MarParCloud campaign. *Atmos. Chem. Phys.*, **20**, 6921–6951, https://doi.org/10.5194/acp-20-6921-2020.

Van Vleet, P. E., and S. M. Williams, 1983: Surface potential and film pressure measurements in seawater systems. *Limnol. Oceanogr.*, **28**, 401–414, https://doi.org/10.4319/lo.1983.28.3.0401.

Veres, P. R., and Coauthors, 2020: Global airborne sampling reveals a previously unobserved dimethyl sulfide oxidation mechanism in the marine atmosphere. *Proc. Natl. Acad. Sci. USA*, **117**, 4505–4510, https://doi.org/10.1073/pnas.1919344117.

Vergara-Temprado, J., and Coauthors, 2017: Contribution of feldspar and marine organic aerosols to global ice nucleating particle concentrations. *Atmos. Chem. Phys.*, **17**, 3637–3658, https://doi.org/10.5194/acp-17-3637-2017.

Vignati, E., and Coauthors, 2010: Global scale emission and distribution of sea-spray aerosol: Sea-salt and organic enrichment. *Atmos. Environ.*, **44**, 670–677, https://doi.org/10.1016/j.atmosenv.2009.11.013.

Wang, Y., C. Shen, J. Li, H. Jiang, and Y. Chu, 2012: Proton transfer reaction mass spectrometry (PTR-MS). *Mass Spectrometry Handbook*, Vol. 109, John Wiley and Sons, 605–630.

Wang, Z. M., and Coauthors, 2016: Contrasting cloud composition between coupled and decoupled marine boundary layer clouds. *J. Geophys. Res. Atmos.*, **121**, 11679–11691, https://doi.org/10.1002/2016JD025695.

Weber, R. J., and Coauthors, 2001: Measurements of enhanced H_2SO_4 and 3–4 nm particles near a frontal cloud during the First Aerosol Characterization Experiment (ACE 1). *J. Geophys. Res.*, **106**, 24107–24117, https://doi.org/10.1029/2000JD000109.

Welti, A., and Coauthors, 2020: Ship-based measurements of ice nuclei concentrations over the Arctic, Atlantic, Pacific and Southern Oceans. *Atmos. Chem. Phys.*, **20**, 15191–15206, https://doi.org/10.5194/acp-20-15191-2020.

Wilson, T. W., and Coauthors, 2015: A marine biogenic source of atmospheric ice-nucleating particles. *Nature*, **525**, 234–238, https://doi.org/10.1038/nature14986.

Wurl, O., L. Miller, and S. Vagle, 2011: Production and fate of transparent exopolymer particles in the ocean. *J. Geophys. Res.*, **116**, C00H13, https://doi.org/10.1029/2011JC007342.

Zäncker, B., A. Bracher, R. Röttgers, and A. Engel, 2017: Variations of the organic matter composition in the sea surface microlayer: A comparison between open ocean, coastal, and upwelling sites off the Peruvian coast. *Front. Microbiol.*, **8**, 2369, https://doi.org/10.3389/fmicb.2017.02369.

Zeppenfeld, S., M. van Pinxteren, M. Hartmann, A. Bracher, F. Stratmann, and H. Herrmann, 2019: Glucose as a potential chemical marker for ice nucleating activity in Arctic seawater and melt pond samples. *Environ. Sci. Technol.*, **53**, 8747–8756, https://doi.org/10.1021/acs.est.9b01469.

Zhang, Z., L. Liu, C. Liu, and W. Cai, 2003: Studies on the sea surface microlayer: II. The layer of sudden change of physical and chemical properties. *J. Colloid Interface Sci.*, **246**, 148–159, https://doi.org/10.1016/S0021-9797(03)00390-4.

Zheng, G., and Coauthors, 2021: New particle formation in the remote marine boundary layer. *Nat. Commun.*, **12**, 527, https://doi.org/10.1038/s41467-020-20773-1.